Revised History of Pleistocene Vertical Motions in NE Sicily and Southern Calabria, Italy, from $^{40}Ar/^{39}Ar$ Dating and Fault Zone Morphology

Rebecca J. Dorsey[1], Gianfranco Di Vincenzo[2], Marco Meschis[3], Sergio G. Longhitano[4], William Cavazza[5], Domenico Chiarella[5]

[1] Department of Earth Sciences, University of Oregon, Eugene, OR, 97403, USA
[2] Istituto di Geoscienze e Georisorse – CNR, via Moruzzi 1, 56124 Pisa, Italy
[3] Istituto Nazionale di Geofisica e Vulcanologia (INGV), Via Ugo La Malfa 153, 90100, Palermo, Italy
[4] Department of Basic and Applied Sciences, Università degli Studi della Basilicata, Viale dell'Ateneo Lucano 10, 85100, Potenza, Italy
[5] Department of Biological, Geological and Environmental Sciences, University of Bologna, Piazza di Porta San Donato 1, 40126 Bologna, Italy

Corresponding author: Rebecca Dorsey (rdorsey@uoregon.edu)

This manuscript is a non-peer-reviewed preprint submitted to EarthArXiv that is currently undergoing review at *Tectonics*.

Key Points:

- A new $^{40}Ar/^{39}Ar$ date on tuff from bathyal marine claystone in northeast Sicily yields an age of 0.481 ± 0.019 Ma.
- The claystone and age-equivalent marl in southern Calabria formed during regional forearc subsidence between ~ 1.0 and 0.5 Ma.
- Widespread post-0.5 Ma marine terraces at elevations up to 1.3 km above sea level record long-term uplift rates faster than 2.5 mm/y.

ABSTRACT

Long-term rates of crustal uplift in southern Calabria and NE Sicily are incompletely understood due to limited information about the age of marine terraces at 1.0–1.3 km above sea level (asl). This study provides a new constraint on high-elevation terrace ages through integrated analysis of geochronology, stratigraphy, shoreline modeling, and fault-zone morphology. $^{40}Ar/^{39}Ar$ step-heating experiments on glass from a tuff in marine claystone of the Argille di Spadafora, NE Sicily, yield reproducible age spectra with a mean age of 0.481 ± 0.019 Ma (± 2σ). The Argille di Spadafora and equivalent marl in southern Calabria are overlain by Pleistocene marine terrace deposits, indicating the terraces are younger than 0.50 Ma. Paleoshoreline modeling at Campo Piale, southern Calabria, suggests an age of 525–590 ka for a terrace at 600–630 m asl: this is an overestimate because it assumes no fault offsets, tilting or structural warping despite geomorphic evidence for these processes. We correlate the 630-m terrace to the marine terrace at 1.0–1.3 km asl based on recognition of a relay ramp between the Cittanova and Sant'Eufemia faults, and geomorphic evidence for fault offset of the terrace. We conclude that marine terraces up to 1.0–1.3 km asl are all < 0.50 Ma, roughly half the widely cited estimate of 1.0 ± 0.2 Ma. The revised age suggests an average uplift rate of > 2.5 mm/y for the highest terrace, and variable throw rates up to 1.0 mm/y on normal faults that cut the terraces.

Plain Language Summary

Tectonic extension in southern Calabria and NE Sicily has produced a network of seismically active normal faults that generate frequent earthquakes accompanied by mantle-driven regional uplift. The timing and rates of uplift in this region are poorly understood due to limited knowledge about the age of Pleistocene marine terraces, up to 1.3 km above sea level, that are cut and offset by normal faults. Because terrace sediments are difficult to date directly, we used $^{40}Ar/^{39}Ar$ isotopic methods to date a volcanic tuff interbedded with marine claystone in NE Sicily that lies stratigraphically below – and is older than – the marine terrace deposits. Laser argon experiments show that the tuff is 0.481 ± 0.019 million years old, providing a precise reliable age of deposition for the claystone. Prior works show that the claystone in Sicily correlates to widespread marine clay and marl in southern Calabria that are overlain by the marine terrace deposits. We therefore conclude that the terraces are younger than 500,000 years old, and the highest terraces are being uplifted at rates > 2.5 mm per year. These results provide a new constraint on models for Pleistocene tectonic evolution, fault interactions, and distribution of uplift in this active region.

1 INTRODUCTION

Southern Italy is a tectonically active region where southeastward retreat of the Ionian subduction zone and migrating tears in the subducting slab drive rapid extension, rifting, and uplift (Fig. 1) (Catalano et al., 2008; Clementucci et al., 2024; Faccenna et al., 2011, 2014; Gallen et al., 2023; Palano et al., 2017; L. Tortorici et al., 1995; Westaway, 1993; Wortel & Spakman, 2000). In southern Calabria, a regional sequence of marine terraces at elevations up to 1.3 km above sea level (asl) are cut and offset by a complex network of seismically active normal faults (Figs. 1, 2). The highest-elevation marine terrace remnants at 1.0–1.3 km asl (Fig. 1) were named SCA terrace for the Serre, Cittanova and Armo faults that cut them (Roda-Boluda & Whittaker, 2017). Several studies have dated terraces at lower elevations (< 200 m asl) using luminescence and radiocarbon methods (e.g., Antonioli et al., 2021; Balescu et al., 1997), but no conclusive independent ages exist for the SCA terrace above 1,000 m asl. As a result, the long-term rates and drivers of uplift in this region remain incompletely understood. Prior studies found that fault-related uplift rates have varied in time and space (Meschis et al., 2022; Quye-Sawyer et al., 2021; Roda-Boluda & Whittaker, 2017), but direct age constraints for Pleistocene marine terraces at elevations ≥ 1.0 km asl remain scarce.

Geomorphic study of extending regions in coastal areas requires testing of alternate hypotheses for the origins and relative ages of marine terraces (Fig. 3). Steep slopes between flat marine terraces may be interpreted as either: (1) paleo-sea cliffs cut by wave action during uniform uplift of an intact crustal block (Fig. 3a); or (2) normal faults that offset a single original terrace where steeper slopes represent fault scarps, the base of each scarp is a hanging wall cut-off, and uplift rate increases landward across each successive fault (Fig. 3b) (Robertson et al., 2020). Most prior studies of marine terraces in southern Calabria have assumed the first model by invoking changes in sea level superposed on an un-faulted uplifting region (Antonioli et al., 2021; Dumas et al., 1981, 1987, 1988, 2005; Miyauchi, 1994; Monaco et al., 2017), despite published evidence that many slopes separating flat terrace surfaces are active normal faults (Figs. 1, 2) (Catalano et al., 2008; Ghisetti et al., 1983; Jacques et al., 2001; Monaco & Tortorici, 2000; Pirrotta et al., 2021, 2022; G. Tortorici et al., 2003; L. Tortorici et al., 1995). In two important exceptions, Catalano et al. (2008) noted offset of the SCA terrace by ~300 m on the Sant'Eufemia fault east of Scilla, and Roda-Boluda and Whittaker (2017) recognized that the SCA terrace is offset up to 500–600 m on the Armo fault southeast of Reggio Calabria (Fig. 1). Other studies describe fault control on variations in elevation of marine terraces

below 200 m asl near Reggio Calabria (Aloisi et al., 2013; Meschis et al., 2022; Monaco et al., 2017), but little progress has been made on this problem at the regional scale since 2017.

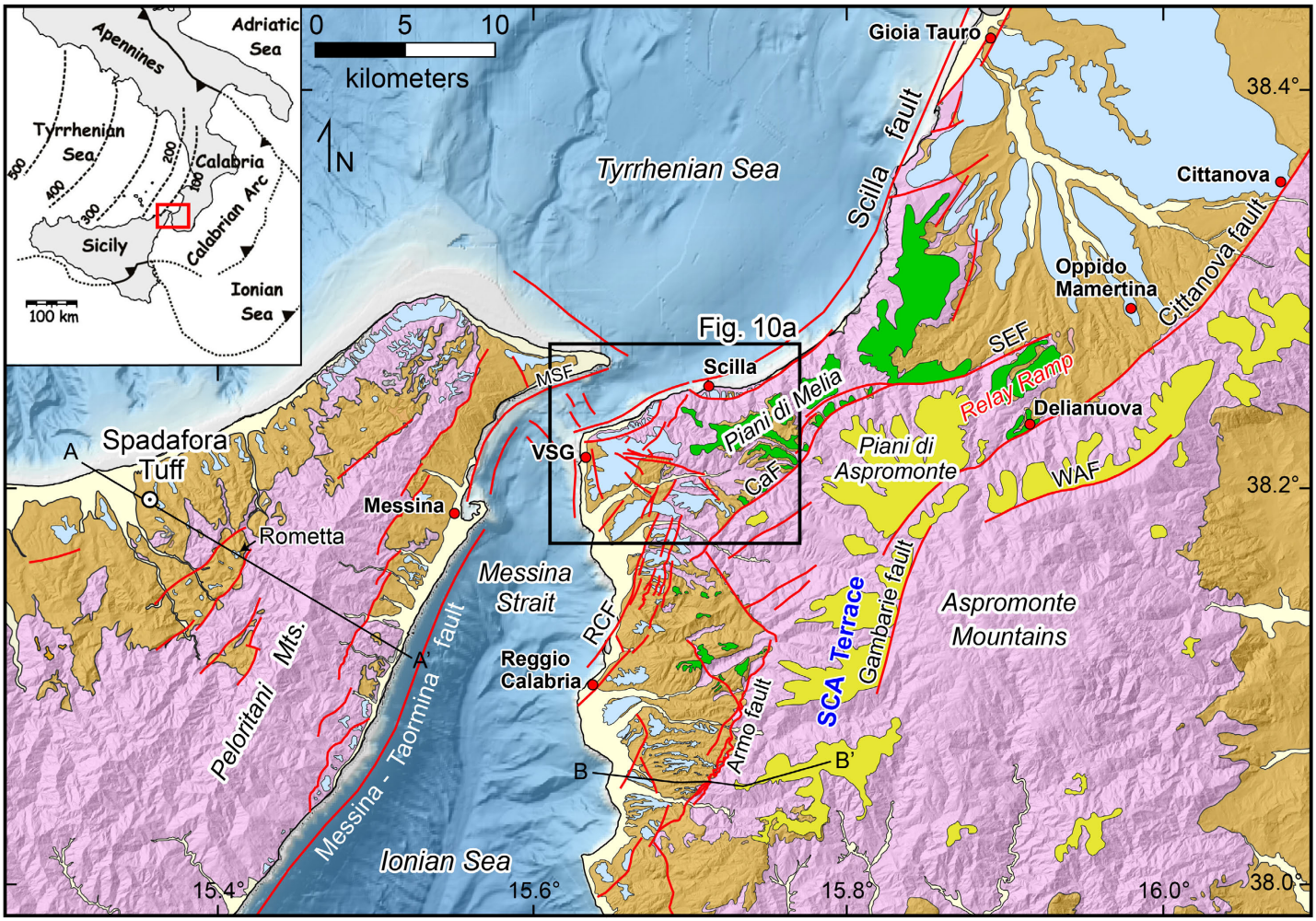

EXPLANATION

- Holocene sediments
- Marine terraces (elevation, m)
  - 900 – 1300
  - 500 – 900
  - 50 – 500
- Miocene-Pleistocene sediments & sedim. rocks
- metamorphic & plutonic basement rocks

Figure 1. Geologic map of southern Calabria and NE Sicily on hillshade topography base, showing marine terraces (colored by elevation bins) and location of the Spadafora tuff. Red lines are normal faults. Note the large relay ramp that accommodates transfer of extensional strain between the Cittanova and Sant'Eufemia faults. Inset: regional tectonic setting (Aloisi et al., 2012) with location of map (red box). Abbreviations: CaF, Calanna Fault; MSF, Messina Strait fault; RCF, Reggio Calabria fault; SEF, Sant'Eufemia fault; VSG, Villa San Giovanni; WAF, Western Aspromonte fault. SCA Terrace is named for the Serre, Cittanova, and Armo faults that cut it (Roda-Boluda and Whittaker, 2017). Geology and faults compiled from Ghisetti et al. (1983), Lentini et al. (2000), Bucci et al. (2022), Lavecchia et al. (2024). Cross sections A-A' and B-B' in Figure 6.

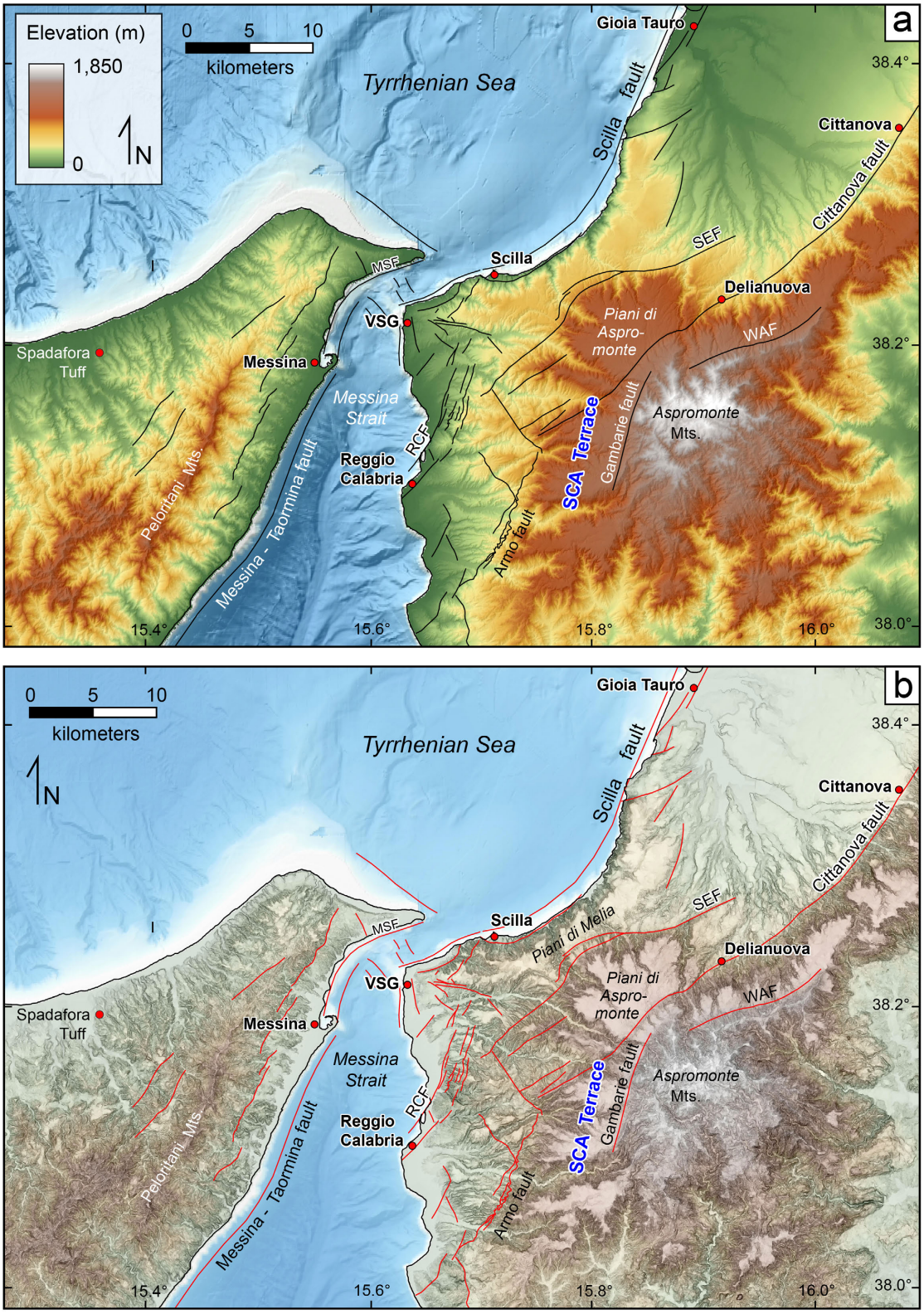

Figure 2. Topography of southern Calabria and NE Sicily, extracted from Tinitaly 10-m digital elevation model (Tarquini et al., 2023). (a) Color Digital Elevation Model (DEM). (b) Slope Map: bright areas represent low slopes, dark areas are steep slopes. Location and abbreviations as in Fig. 1.

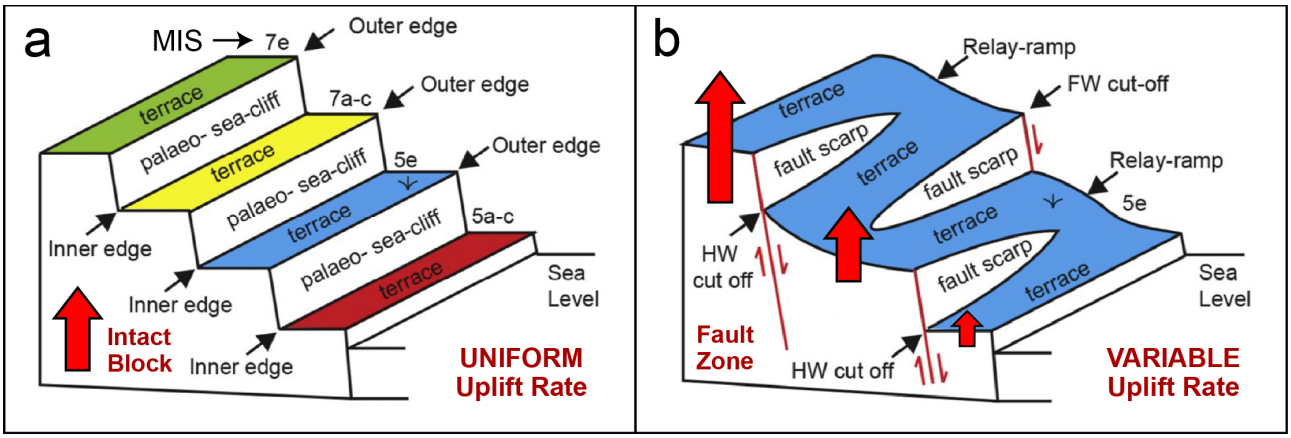

Figure 3. Alternate hypotheses to explain the origin and relative ages of uplifted marine terraces. (a) Paleo-sea cliffs cut by wave action during uniform uplift of an intact, un-faulted crustal block during multiple cycles of glacioeustatic sea-level change. MIS is marine isotope stage. (b) Offset of a single original terrace by multiple normal faults: steep slopes are interpreted as fault scarps, the base of each scarp is a hanging wall cut-off, and uplift rate (red block arrows) increases landward across successive fault strands. Modified from Robertson et al. (2020).

This study uses the $^{40}Ar/^{39}Ar$ laser method to temporally constrain emplacement of a volcanic tuff interbedded in Pleistocene marine claystone (Argille di Spadafora) of NE Sicily, which correlates to bathyal marine marl (Argille di Vito Superiore) in southern Calabria. The regional claystone-marl unit is overlain by the Messina Gravels and Sands Formation (MGS), which is capped by Pleistocene marine terrace deposits. We integrate the tuff age with regional stratigraphy, paleoshoreline modeling in southern Calabria, and structural-geomorphic analysis of the normal fault network to derive a reliable maximum age for the marine terraces. Our data indicate that the high SCA terrace is < 0.50 Ma, providing a new constraint on the timing and long-term rates of uplift in this region.

2 TECTONIC and GEOLOGIC SETTING

2.1 Tectonic Overview

Southern Calabria and NE Sicily lie within a region of rapid NW–SE extension driven by slab rollback and southeastward retreat of the Ionian subduction zone (Fig. 1) (Faccenna et al., 2011, 2014; Palano et al., 2017; Rosenbaum & Lister, 2004; Wortel & Spakman, 2000). These tectonic motions have produced a complex network of active normal faults that are sources of frequent earthquakes, making this one of the highest seismic hazard areas in the Mediterranean basin. Rapid uplift, erosion and extension in Calabria are widely interpreted to be driven by mantle processes such as migrating slab tears and mantle convection (Clementucci et al., 2024; Faccenna et al., 2011; Gallen et al., 2023;

Quye-Sawyer et al., 2021; Westaway, 1993). Forearc crust in the study area consists of metamorphic and plutonic rocks that form thrust nappes and ophiolite-bearing tectonic units of the Alpine internal zone (Cirrincione et al., 2015; Rossetti et al., 2001; Vitale & Ciarcia, 2013). Crystalline basement and overlying Miocene to Pleistocene sedimentary rocks are cut by normal faults of the Siculo-Calabrian rift zone (Brutto et al., 2016; Catalano et al., 2008; Jacques et al., 2001; Monaco et al., 1997; Monaco & Tortorici, 2000; Pirrotta et al., 2021, 2022; G. Tortorici et al., 2003; L. Tortorici et al., 1995). The modern Messina Strait is a narrow marine connection between the Tyrrhenian and Ionian seas that is maintained by extension and opening between Sicily and Calabria at a rate of ~3 mm/y (Catalano et al., 2008; Serpelloni et al., 2010). Normal faults bounding the Messina Strait define an active conjugate relay zone (*sensu* Childs et al., 2019), where extensional strain is transferred from NW-dipping normal faults in the northeast (southern Calabria) to the SE-dipping Messina-Taormina fault offshore eastern Sicily in the south (Fig. 1; Dorsey et al., 2024).

The Siculo-Calabrian rift zone is a complex network of NE-striking seismically active normal faults in southern Calabria and NE Sicily that accommodate NW-SE extension in the upper plate of the southeast-migrating Ionian subduction zone (Figs. 1, 2) (Catalano et al., 2008; Catalano & De Guidi, 2003; Cavazza & Longhitano, 2023; Jacques et al., 2001; Monaco et al., 1997; Monaco & Tortorici, 2000; Neri et al., 2020; Palano et al., 2012, 2017; Pirrotta et al., 2021, 2022; Presti et al., 2019; G. Tortorici et al., 2003; L. Tortorici et al., 1995). Tortorici et al. (1995) proposed that modern normal faulting may reflect a new rifting process that has developed since Middle Pleistocene time, and that subduction of the Ionian plate is no longer active. The 60-km long Messina-Taormina fault forms the steep western margin of the Messina Strait and likely was the source of the 1908 M7.1 Messina earthquake (Meschis et al., 2019, 2022; Pavano, 2025; Stewart et al., 1997), though some workers propose different models (Aloisi et al., 2013; Argnani, 2021, 2022; Argnani et al., 2009; Barreca et al., 2021). Crystalline basement rocks in the Peloritani Mountains of NE Sicily are undergoing rapid uplift and erosion in the footwall of the Messina-Taormina fault (Catalano & De Guidi, 2003; Monaco & Tortorici, 2000; Pavano, 2025; Pavano et al., 2016, 2024). In contrast to the Messina-Taormina fault, faults in southern Calabria are shorter (1 to 26 km), more numerous, and more closely spaced (0.5 to 5 km) (Fig. 1). The larger faults in southern Calabria (Armo, Reggio Calabria, Scilla, Cittanova, and Sant'Eufemia faults) display along-strike slip gradients with offset increasing toward fault centers and decreasing toward fault tips to produce domal footwall uplifts and lateral throw gradients (Dorsey et al., 2024). Pleistocene to Holocene uplift in southern Calabria

is recorded in Pleistocene marine terraces at elevations up to 1.3 km asl (Antonioli et al., 2006; Dumas et al., 1988, 2005; Dumas & Raffy, 2006; Faccenna et al., 2011; Ferranti et al., 2006, 2007; Ghisetti, 1981; Miyauchi, 1994; Roda-Boluda & Whittaker, 2017; Westaway, 1993).

Southern Calabria has experienced many destructive historical earthquakes on seismically active normal faults, including 19 events of magnitude ≥6 since 91 B.C. (Andrenacci et al., 2023; Galli et al., 2008; Galli & Bosi, 2002). The seismic sequence of 1783 included 5 mainshocks with Mw > 6 in less than 2 months, followed by numerous smaller events spanning 3 years (Andrenacci et al., 2023; Sgambato et al., 2023). The 1783 sequence started on the 5th of February with surface ruptures of magnitude M~7 on the Cittanova and Sant'Eufemia faults, with coseismic displacements stepping across a relay ramp that accommodates transfer of strain between the two faults (Fig. 1; Jacques et al., 2001; Sgambato et al., 2023). The February 5 event increased stresses on the nearby Scilla fault and triggered the M-6.5 Scilla earthquake on February 6. The combined effect of the first two earthquakes produced further stress loading that triggered M6 to M7 earthquakes on the Serre and Vibo faults (~25–45 km north of the study area) in February and March of 1783 (Jacques et al., 2001; Sgambato et al., 2023). In 1908 during the most recent major cycle, the Mw 7.1 Messina earthquake destroyed the cities of Messina and Reggio Calabria inflicting a death toll of >80,000 (Baratta, 1910; Boschi et al., 1989; Monaco & Tortorici, 2000). The damage was amplified by coseismic subsidence and a regional tsunami that inundated coastal areas on both sides of the Messina Strait (Argnani et al., 2009; Barreca et al., 2021; Billi et al., 2008, 2009; Comerci et al., 2015; Favalli et al., 2009). A macroseismic analysis of strong earthquakes in southern Calabria identified three distinct earthquake cycles since 1600 that have produced ~2–4 m of total displacement on regional normal faults in the past ~400 years (Andrenacci et al., 2023). Uplifted Holocene shorelines record four earlier earthquake cycles involving at least 16 strong earthquakes between ~ 6.5 and 1.0 ka (Ferranti et al., 2017). These studies demonstrate rapid fault-slip rates and high seismic hazard in the region.

2.2 Neogene Stratigraphy

Neogene deposits exposed on the Sicilian and Calabrian sides of the Messina Strait (Fig. 1) record the tectonic and sedimentary response to southeast migration of the Ionian subduction zone and related opening of the southern Tyrrhenian basin (Di Stefano et al., 2007; Di Stefano & Lentini, 1995; Lentini et al., 2000; Ogniben, 1960; Vitale & Ciarcia, 2013). Cenozoic terrigenous successions of the Messina Strait region form depositional cycles bounded by regional unconformities that mark

distinct phases in a polyphase tectonic evolution (Fig. 4; Guarnieri et al., 2004; Lentini et al., 1995; Monaco et al., 1996; Zecchin et al., 2015). Upper Oligocene to Miocene turbidites occupy perched forearc and trench-slope basins separated by metamorphic and plutonic basement highs (e.g., Rohais et al., 2021). These strata are overlain along an angular unconformity by Messinian evaporite deposits (on the Sicilian side only), transgressive Lower Pliocene marls (Trubi Fm), and mid-to-upper Pliocene marls and sands (Fig. 4).

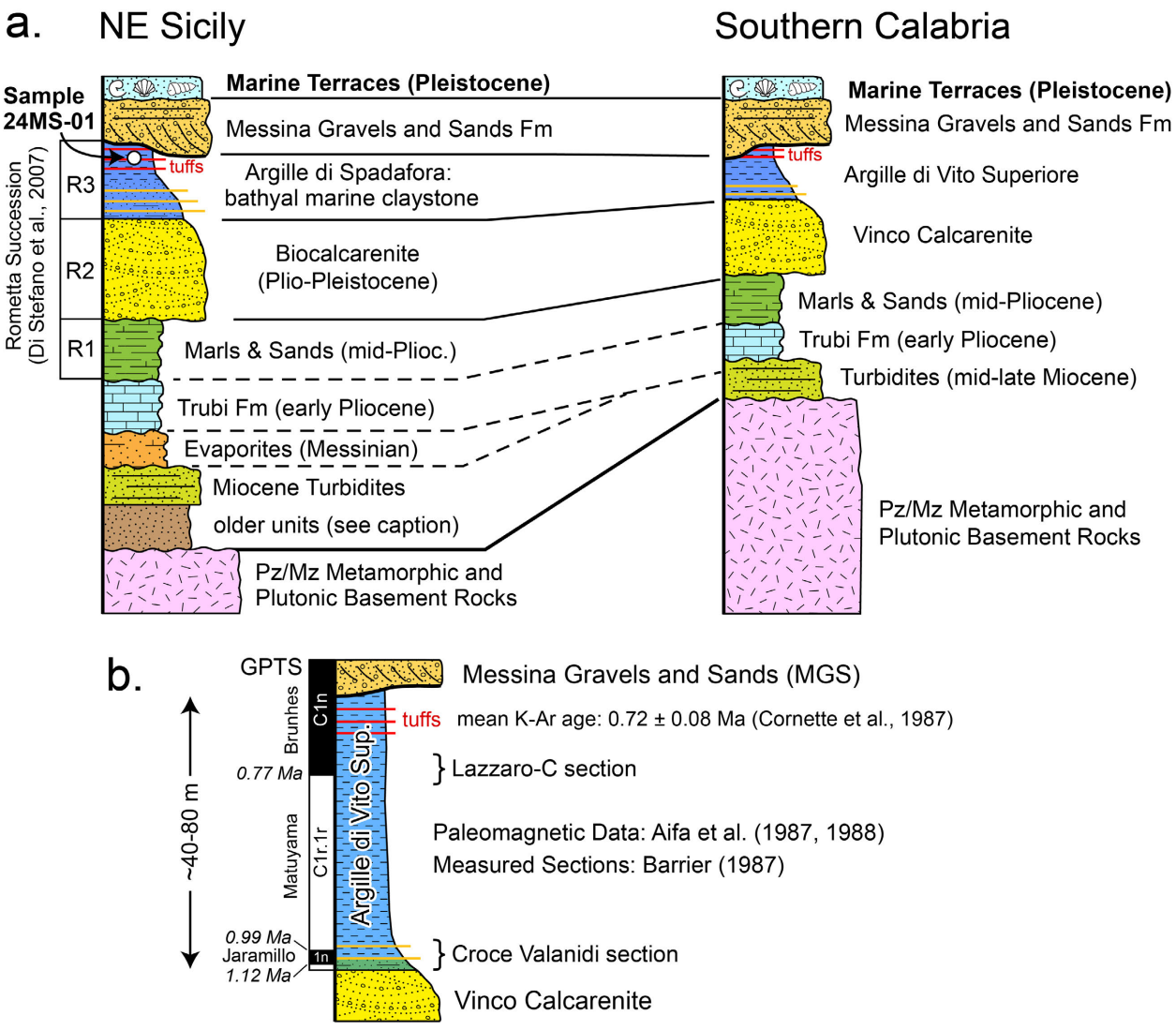

Figure 4. a. General stratigraphy of Miocene – Pleistocene sediments in NE Sicily and southern Calabria, showing position of sample 24MS-01 (this study) and correlation across the Messina Strait (Fig. 1). Not to scale. "Older units" in NE Sicily include the Capo d'Orlando Formation and Floresta Calcarenites. b. Expanded view of Argille di Vito Superiore in southern Calabria with summary of existing age constraints from paleomagnetism (Aïfa et al., 1987, 1988; Barrier, 1987) and K-Ar dates on glass from interbedded tuffs (Cornette et al., 1987). GPTS is geomagnetic polarity timescale (ages from Ogg, 2020).

The Vinco Calcarenite in southern Calabria consists of up to 250 m of cross-stratified bioclastic and siliciclastic tidal sandstones with minor conglomerates, breccias, and mudstones (Fig. 4a; Barrier, 1987; Chiarella et al., 2021; Di Stefano et al., 2007; Di Stefano and Lentini, 1995; Lentini et al., 2000; Longhitano, 2018; Ogniben, 1960). This unit and correlative deposits in NE Sicily (Di Stefano et al., 2007; Di Stefano & Longhitano, 2009; Messina et al., 2009) record tide-dominated sedimentation in the Messina Strait region that persisted from the Gelasian (~2.5 Ma) to mid–late Calabrian (Emilian–Sicilian, ~1.2 Ma) (Barrier, 1984; Di Stefano et al., 2007; Di Stefano & Longhitano, 2009; Lentini et al., 2000; Longhitano et al., 2012; Mercier et al., 1987).

Pleistocene calcarenites are conformably overlain by a widespread 40–80 m thick unit of bathyal marine claystone and marl with interbedded tuffs in the upper part, known as Argille di Spadafora in NE Sicily (Carbone et al., 2022; Lentini et al., 2000) and Argille di Vito Superiore in southern Calabria (Fig. 4b) (Barrier, 1987; Carbone et al., 2022; Di Geronimo et al., 1997; Ghisetti, 1981; Jacques et al., 2001). The clays and marls accumulated during a period of accelerating subsidence, deepening, and widening of the basin (Longhitano, 2018) in water depths of ~500–700 m for the Argille Spadafora (Messina et al., 2009; Di Stefano et al., 2007; Violanti, 1989; Violanti D. et al., 1987) and 500–1000 m for the Argille di Vito Superiore in Calabria (Di Geronimo et al., 1997; Girone, 2003). Calcareous nannofossils include *Pseudoemiliania lacunosa*, *Gephyrocapsa oceanica*, and *Gephyrocapsa sp.3* indicative of biozone MNN19f (Di Stefano et al., 2007; Di Stefano & Lentini, 1995; Lentini et al., 2000; Pino, Baldanza, et al., 2007; Pino, Belfiore, et al., 2007; Rio et al., 1990). This biozone was recently revised to subzone MNQ19d with an established age range of 960–460 ka in the Mediterranean region (Di Stefano et al., 2023).

Cornette et al. (1987) dated volcanic tuffs in Argille di Spadafora and Argille di Vito Superiore using radioisotopic methods. They obtained K–Ar ages from ~1 to 5 Ma on plagioclase separates from tuffs in both formations, but concluded that these ages were unreliable due to low K contents and the likely presence of extraneous Ar. They also obtained a mean K–Ar age of 0.72 ± 0.08 Ma on glass from a tuff in Argille di Vito Superiore at Archi near the coast in southern Calabria, which they assigned a higher level of confidence. Aïfa et al. (1988, 1987) conducted paleomagnetic analysis of clays and marls in Argille di Vito Superiore from several sections southeast of Reggio Calabria (Barrier, 1987). They recognized a stratigraphically defined normal-polarity interval at the base of this unit that they interpreted as the Jaramillo subchron (1.12 to 0.99 Ma; Ogg, 2020), and a reversed-to-normal polarity transition near the top that was assigned to the base of the Brunhes chron (0.77 Ma; Fig. 4b).

Regional correlation of interbedded tuff sequences in the upper part of the clay-marl unit, combined with its limited thickness (< 100 m) and results of this study (below), indicate that bathyal conditions prevailed over a large region between ~ 1.0 and 0.5 Ma.

The Messina Gravels and Sands Formation (MGS; Fig. 4) unconformably overlies older deposits and records a subsequent period of coarse sediment input from adjacent mountains and progradation of gravelly fan deltas into the Messina Strait (Barrier, 1987; Di Stefano & Lentini, 1995; Ghisetti et al., 1983; Mercier et al., 1987; Ogniben, 1960). Pavano et al. (2024) obtained luminescence ages of ~330–200 ka for MGS near the coast of NE Sicily ~25 km south of our sample site 24MS-01 (Fig. 1). MGS Gilbert deltas range from 12 to 180 m thick and include dipping foresets that prograded over bottomsets of the underlying marine clay and marl units (Barrier et al., 1986; Barrier & D'Alessandro, 1985). MGS foresets are overlain by flat-lying topset facies of fossiliferous shallow marine to coastal and terrestrial sands and gravels. The age of MGS is widely attributed to the late Middle Pleistocene, with field evidence indicating that deltaic units become younger toward the strait axis (Longhitano, 2018). The amount of time missing at the unconformable base of MGS is not known, while the conformable contact between MGS and overlying marine terrace sediments suggests continuous deposition.

2.3 Pleistocene Marine Terraces

Marine terraces cap Neogene sediments in southern Calabria at elevations from ~50 m to 1,300 m asl (Figs. 1, 4; Antonioli et al., 2021; Miyauchi, 1994; Monaco et al., 2017; Roda-Boluda and Whittaker, 2017). Terrace deposits vary from fossiliferous sands to non-fossiliferous gravels and sands that rest on older units ranging from crystalline basement rock to Miocene, Pliocene and Pleistocene sedimentary deposits (Fig. 1). Balescu et al. (1997) dated marine terrace deposits from several localities in the Reggio Calabria area using thermoluminescence methods. They obtained an age of 64 ± 8 ka for non-fossiliferous eolian sand from a raised marine terrace ~40 m asl in Villa San Giovanni (Fig. 1). This terrace most likely corresponds to Marine Isotope Stage (MIS) 3c (50 ka; Siddall et al., 2003; Rohling et al., 2014), suggesting an uplift rate of ca. 0.8 mm/y since 50 ka, generally consistent with other investigations in the Campo Piale area (Antonioli et al., 2021; Monaco et al., 2017). Marine terraces assigned to MIS 5e (125 ka) that formed during the Last Interglacial Maximum have been mapped at elevations of ~100 to 200 m asl from Villa San Giovanni to Reggio Calabria (Balescu et al., 1997; Dumas et al., 1988, 2005; Ferranti et al., 2006, 2007; Meschis et al., 2022;

Miyauchi, 1994). Marine terraces of this age contain fossils including *Persististrombus latus*, previously known as "*Strombus bubonius*" (Cerrone et al., 2021). These fossils are considered diagnostic of MIS 5e (125 ka; Balescu et al., 1997) and are common in terraces between 120 and 180 m asl south of Reggio Calabria (Balescu et al., 1997; Dumas et al., 1988, 2005). The large variability in elevation of the MIS 5e terrace over short distances has been attributed to Late Pleistocene fault offsets on the Reggio Calabria and Armo faults (e.g., Aloisi et al., 2013; Meschis et al., 2022).

A review of previous studies in paleontology (Barrier et al., 1986; Miyauchi, 1994), geochronology (Cornette et al., 1987), and coastal terraces (Dumas et al., 1981, 1987, 2005) suggested that the high SCA terrace has a likely age of 1.0 ± 0.2 Ma (Roda-Boluda & Whittaker, 2017). Subsequent studies have used this age to constrain the timing and distribution of regional uplift, calculate fault-throw rates, calibrate model-based erosion rates, and interpret landscape response to active faulting in southern Calabria (Clementucci et al., 2024; Quye-Sawyer et al., 2021; Robustelli, 2019; Roda-Boluda et al., 2018, 2019; Roda-Boluda & Whittaker, 2017; Sgambato et al., 2023). Some studies find that extension and normal faulting started after deposition of the marine terrace sediments (Catalano et al., 2008; Jacques et al., 2001; L. Tortorici et al., 1995), while others conclude that normal faults were active earlier during deposition of the Vinco Calcarenite and MGS (e.g., (Barrier, 1986; Chiarella et al., 2021; Ghisetti et al., 1983). Our review of the literature indicates that normal faults initiated during deposition of the Vinco Calcarenite and likely were active before, during, and after deposition of Pleistocene marine terraces in the study area (Fig. 1).

3. METHODS

3.1 $^{40}Ar/^{39}Ar$ Geochronology

Tuff unit VU7 was identified in the field using the published base map and stratigraphic nomenclature of Di Bella et al. (2016), and a fresh sample of the tuff was collected for $^{40}Ar/^{39}Ar$ geochronology. $^{40}Ar/^{39}Ar$ analyses were performed at IGG–CNR (Pisa, Italy) using both the laser step-heating and the laser total fusion techniques. Glass and plagioclase separates were obtained using standard separation techniques followed by careful handpicking under a stereomicroscope. Plagioclase separate was leached for a few minutes in an ultrasonic bath using HF 7% at room temperature. Glass separate was cleaned by alternating methanol and deionized water. Back-scattered electron imaging of the glass separate was acquired at IGG–CNR by a field emission scanning electron microscope (FE-SEM) Zeiss Sigma 360 VP, using an acceleration voltage of 10 kV

and a working distance of 8.5 mm. Separates were wrapped in aluminum foil and irradiated along with the Alder Creek sanidine (ACs) in the core of the TRIGA reactor at the Università di Pavia (Italy) in two distinct batches of 3 hours in duration: PAV-95 in September 2024 and PAV-96 in February 2025. The neutron fluence was monitored by analyzing single grains of the ACs reference material, which were melted using a continuous wave CO_2 laser (ESL MIR10^2 CO_2 laser system). The laser beam was homogenized using a beam expander and a top-hat beam shaper lens. Total fusion analyses were completed on individual crystals of plagioclase from the 0.5–1.0 mm fraction and on three grains of glass (0.25–0.50 mm fraction), which were placed onto the bottom of 1.5-mm diameter holes of a copper holder. Aliquots of 10–20 mg for plagioclase and of ~5–6 mg for glass were also laser step heated using the same CO_2 laser as above. Samples were placed onto the bottom of 6-mm diameter holes of a copper holder as a single layer and the laser beam, defocused to 2-mm spot size, was automatically slowly rastered (at 0.2 mm/s) over the separate. Steps were carried out at increasing laser power until complete melting. Prior to $^{40}Ar/^{39}Ar$ analyses, the copper holder was loaded into a vacuum chamber comprising a laser port consisting of a ZnSe window fitted with a differentially pumped flange, and baked for 15 h at 150°C. In order to reduce atmospheric Ar contamination, total fusion analyses of separates from the second irradiation were pre-heated for 30 s at 0.15 W laser power and using the laser beam defocused to 2-mm spot.

Argon isotope compositions were acquired simultaneously using a multi-collector noble gas mass spectrometer ARGUS VI (Thermo Fisher Scientific). Ar isotopes from 40 to 37 were acquired using Faraday detectors, equipped with 10^{13} Ω amplifier resistors. Faraday detectors were cross calibrated for the slight offset using air shots. ^{36}Ar was measured using a low-noise CuBe Compact Discrete Dynode (CDD) detector. Gas purification for total fusion experiments was achieved using one water cooled SAES NP10 getter held at ~400° C and one SAES C-50 getter held at room temperature. For step-heating analyses, gas purification included an additional AP10 getter held at ~400° C and a cryogenic condensation trap using an ethanol-dry ice mixture. Blanks were monitored every two runs and were subtracted from succeeding sample results. Line blanks are given in the data repository (Di Vincenzo et al., 2025). More details about mass spectrometer calibration and analysis can be found in Di Vincenzo et al. (2021) and Di Vincenzo (2022). Ages were calculated using decay constants recalculated by Min et al. (2000), an atmospheric $^{40}Ar/^{36}Ar$ ratio of 298.56 ± 0.3160 (Lee et al., 2006) and an age of 1.1848 ± 0.0012 Ma for the Acs (Niespolo et al., 2017). Data corrected for post-irradiation decay, mass discrimination effects and blanks (relative abundances) are listed in the online

data repository (Di Vincenzo et al., 2025). Uncertainties on the ages from single runs are 2σ analytical uncertainties, including in-run statistics and uncertainties in the discrimination factor, interference corrections and procedural blanks. Uncertainties on error-weighted means also include the uncertainty on the fluence monitor (2σ internal errors).

3.2 Synchronous Correlation Approach to Paleoshoreline Modelling

The synchronous correlation method was developed by Houghton et al. (2003) and Roberts et al. (2009, 2013) and applied in several investigations to derive terrace ages and uplift rates in the Mediterranean realm and elsewhere (Cerrone et al., 2025; De Santis et al., 2023; Meschis et al., 2018, 2020, 2022; Pedoja et al., 2018; Robertson et al., 2019, 2023; Varzi et al., 2024). This approach has been explained previously (Houghton et al., 2003; Roberts et al., 2009, 2013) and is summarized here. The synchronous correlation method is based on the idea that late Quaternary sea-level highstands, which produce uplifted sea-level indicators such as marine terraces and coastal notches, are unequally spaced in time. This implies that sea-level indicators should be unequally spaced in elevation for uniform uplift rates, which enables the user to test scenarios for constant versus variable uplift rates through time (Cerrone et al., 2025; Meschis et al., 2022, 2024; Roberts et al., 2009, 2013; Robertson et al., 2019, 2023). This approach also addresses the "re-occupation" problem where younger sea-level indicators may be superposed on older ones, and thus avoid assigning erroneous ages to undated sea-level indicators in regions of relatively slow uplift. In this method, the simplest hypothesis for constant uplift rate is examined by iterating uplift rates constrained by one or more age controls from literature or newly obtained with absolute dating. We iteratively calculate predicted sea-level highstand elevations and assess whether the predicted elevations match the elevations of observed (mapped) terraces. If a robust match is not obtained, then scenarios with changing uplift rate through time are explored to minimize the mismatch between predicted and observed terrace elevations (e.g., Meschis et al., 2022; Roberts et al., 2009).

Paleoshoreline modelling for this study assumes sea-level highstand ages and elevations from well-established Quaternary sea-level curves (Rohling et al., 2014; Siddall et al., 2003) (Table 1). We execute synchronous correlation of mapped and predicted paleoshoreline elevations using a "Terrace Calculator" built in Excel (Table S1) where uplift rate, sea-level highstand ages, and elevations are used as input data (e.g., Cerrone et al., 2025; De Santis et al., 2025, 2023, 2021; Roberts et al., 2013; Robertson et al., 2023, 2019). We seek to correlate the geomorphologically most distinct inner edges

of marine terrace treads (picked at slope inflections from the 10-m DEM) with the most prominent sea-level highstands mapped in the Mediterranean region, including MIS 5e (125 ka), MIS 7e (240 ka) and MIS 9e (340 ka). We also assess the presence of other less prominent marine terraces such as MIS 3c (50 ka), MIS 5a (77 ka), MIS 5c (100 ka), MIS 9c (310 ka), MIS13–15 (478–590 ka). In this study, we use two reliable age controls available in the Campo Piale area: (1) a paleoshoreline at ~40 m asl in Villa San Giovanni (Balescu et al., 1997) that we assign to 50 ka based on the Mediterranean sea-level chronology (Rohling et al., 2014; Siddall et al., 2003); and (2) a prominent terrace at ~125 to 180 m elevation with a widely accepted age of 125 ka (MIS 5e) (e.g. Dumas et al; Monaco et al., 2017; Antonioli et al., 2021). We then produce linear regressions to assess the correlation between measured and predicted paleoshoreline elevations, seeking to maximize the R^2 value. The margin of uncertainty associated with paleoshoreline elevations mapped with the DEM is ± 10 m. Sea-level curves used in this study have a margin of uncertainty of ± 12 m (Siddall et al., 2003) and 6 m (Rohling et al., 2014). The margin of error for the age of sea-level highstands is ± 4 ky for both sea-level curves used in this study (Meschis et al., 2024; Rohling et al., 2014; Siddall et al., 2003).

3.3 Geomorphic Analysis of Normal Faults

Normal faults were compiled from published geologic maps (Bucci et al., 2022; Ghisetti et al., 1983) and a digital fault database (Lavecchia et al., 2024). We used the Tinitaly/1.1 10-m digital elevation model (Tarquini et al., 2023; https://tinitaly.pi.ingv.it/) to plot geomorphic features in QGIS, supplemented with field observations and 3D visualization in Google Earth Pro®. Our analysis is based on existing knowledge of the geometries, interactions, and evolution of extensional normal fault networks. Geometries indicative of deformation and erosion processes include triangular facets, wineglass-shaped canyons, relay ramps, conjugate relay zones, along-strike changes in fault throw, strain gradients, and transfer faults (Childs et al., 2019; Cowie et al., 2000; Cowie & Roberts, 2001; Finch & Gawthorpe, 2017; Fossen & Rotevatn, 2016; Goldsworthy & Jackson, 2000, 2001; Holtmann et al., 2023; Khalil & McClay, 2017; Mearns & Sornette, 2021; Pan et al., 2022; Peacock & Sanderson, 1991, 1994; Petit et al., 2009; Roche et al., 2021; Rotevatn et al., 2019; Tucker et al., 2011, 2020; Walsh et al., 2001). Identification of fault-related geomorphic features such as triangular fault facets and intervening steep wineglass canyons (e.g., Stewart and Hancock, 1988; Tucker et al., 2020, 2011; Wallace, 1977) allows us to test alternate hypotheses for the origins and relative ages of uplifted marine terraces (Fig. 3; Robertson et al., 2020).

4. RESULTS

4.1 Geology of Pleistocene Marine Terraces

Pleistocene terraces form large low-gradient surfaces that occupy a wide range of elevations from ~100 to 1,300 m asl in southern Calabria, with smaller scattered erosional remnants in NE Sicily (Figs. 1, 2). Terrace deposits rest either on older sediments or an erosional strath beveled on crystalline basement, and consist of ~5–50 m-thick deposits capped by a thin red soil and truncated by steep eroding valleys and canyons (Fig. 5a). Sedimentary lithofacies include uncemented well-sorted beach sands (Fig. 5b), stratified pebbly gravels and sands (Fig. 5c), variably cemented shelly fossiliferous sands (Figs. 5d, 5e), carbonate-cemented shell beds (sandy limestone) interbedded with less well cemented siliciclastic sands and gravels, red fluvial sands and gravels, and minor poorly sorted matrix-rich gravels close to fault scarps. In some areas, Gilbert-delta topsets of MGS are conformably overlain by – and indistinguishable from – Pleistocene terrace deposits (Fig. 5c). Pleistocene terrace deposits and underlying units are offset by numerous active normal faults in the study area (Figs. 1, 6). In NE Sicily, the faulted section consists of metamorphic and plutonic basement overlain by Miocene sedimentary rocks, Pleistocene marine calcarenites, Argille di Spadafora, MGS, and capping marine to fluvial terraces that are down-dropped ~300 m in a fault-bounded graben in the Rometta area (Fig. 6a). The presence of numerous young normal faults, combined with partial preservation to absence of sedimentary rocks in uplifted footwall blocks, suggests the Cenozoic succession has been removed by erosion along the crest of the Peloritani Mountains. The sediments could have onlapped metamorphic basement if topography was present during deposition, but no evidence for this relationship is preserved in the rock record. In southern Calabria, the geologic cross section reveals ~1,000 m total displacement on the Armo fault with a 300–400-m thick Cenozoic section in the hanging wall that is absent in the footwall. The capping Pleistocene marine terrace is offset ~500 m on the Armo fault (Fig. 6b), as previously documented by Roda-Boluda and Whittaker (2017). East of the Armo fault in the footwall, SCA terrace deposits rest on crystalline basement rock and a thin discontinuous interval of Vinco Calcarenite. The SCA marine terrace in the hanging wall of the Armo fault dips ~3–5° west, away from the fault, and projects down-dip toward sands at ~100 m asl that were dated at ~125 ka by Balescu et al. (1997) (Fig. 6b).

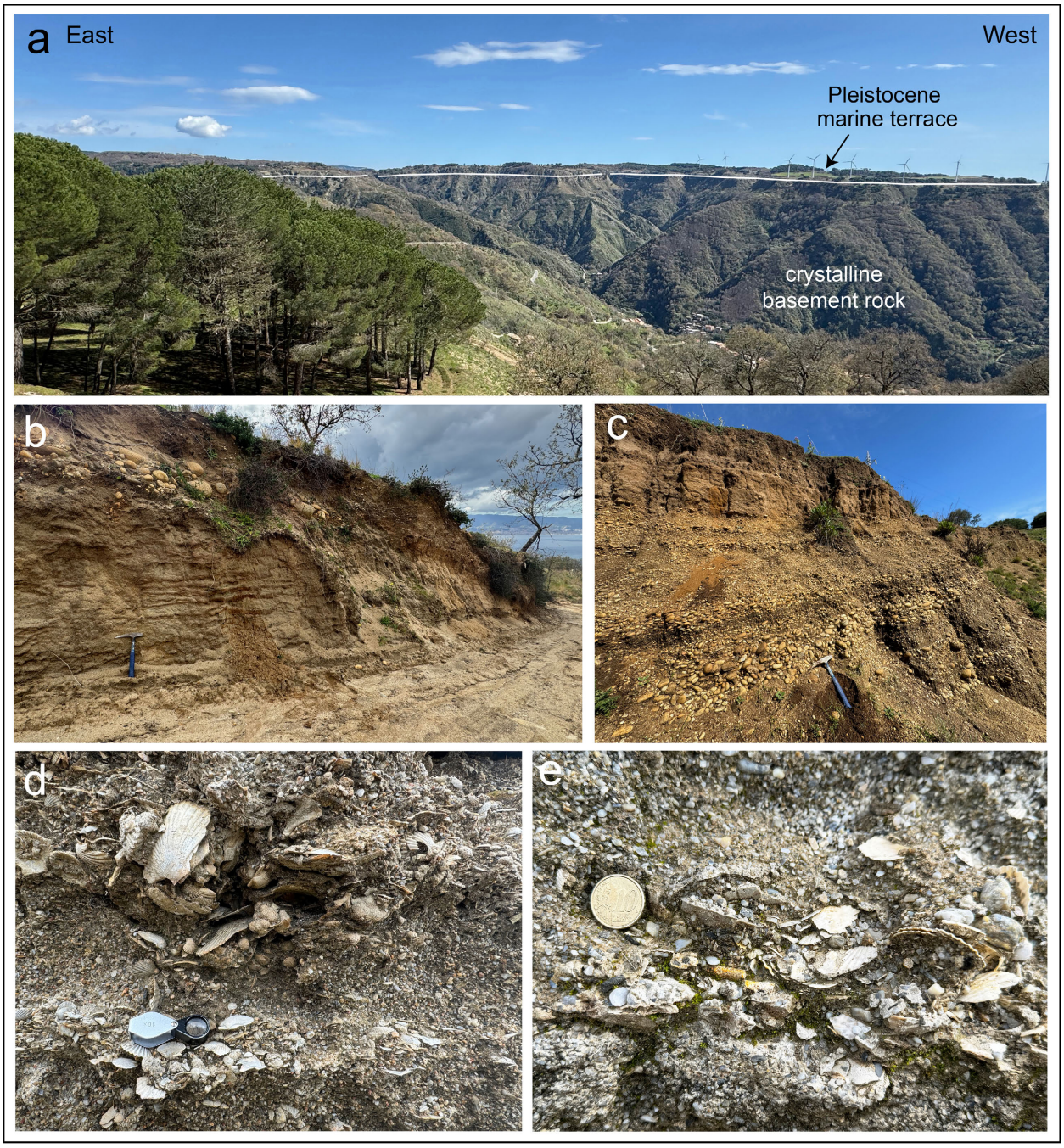

Figure 5. Field photos of Pleistocene marine terraces and related deposits in southern Calabria. (a) View looking south at the high SCA terrace at ~1,000 m elevation in the footwall of the Armo fault. (b) Uncemented well sorted beach sands at ca. 375 m elevation in a small erosional remnant of the Pleistocene marine terrace in the Reggio Calabria fault zone north of Reggio Calabria. (c) Well stratified beach gravels and sands in topsets of the Messina Gravels and Sands Formation directly beneath capping soils of the Pleistocene terrace at ~150 m elevation east of Villa San Giovanni. (d) Close-up of fossiliferous sands in a terrace remnant at 375 m elevation in the Reggio Calabria fault zone. (e) Close-up of fossiliferous sands at 955 m elevation in footwall of the Armo fault, showing strong resemblance to other Pleistocene terrace sands at elevations ranging from 100 to 1,000 m asl in southern Calabria. Referenced locations in Fig. 1.

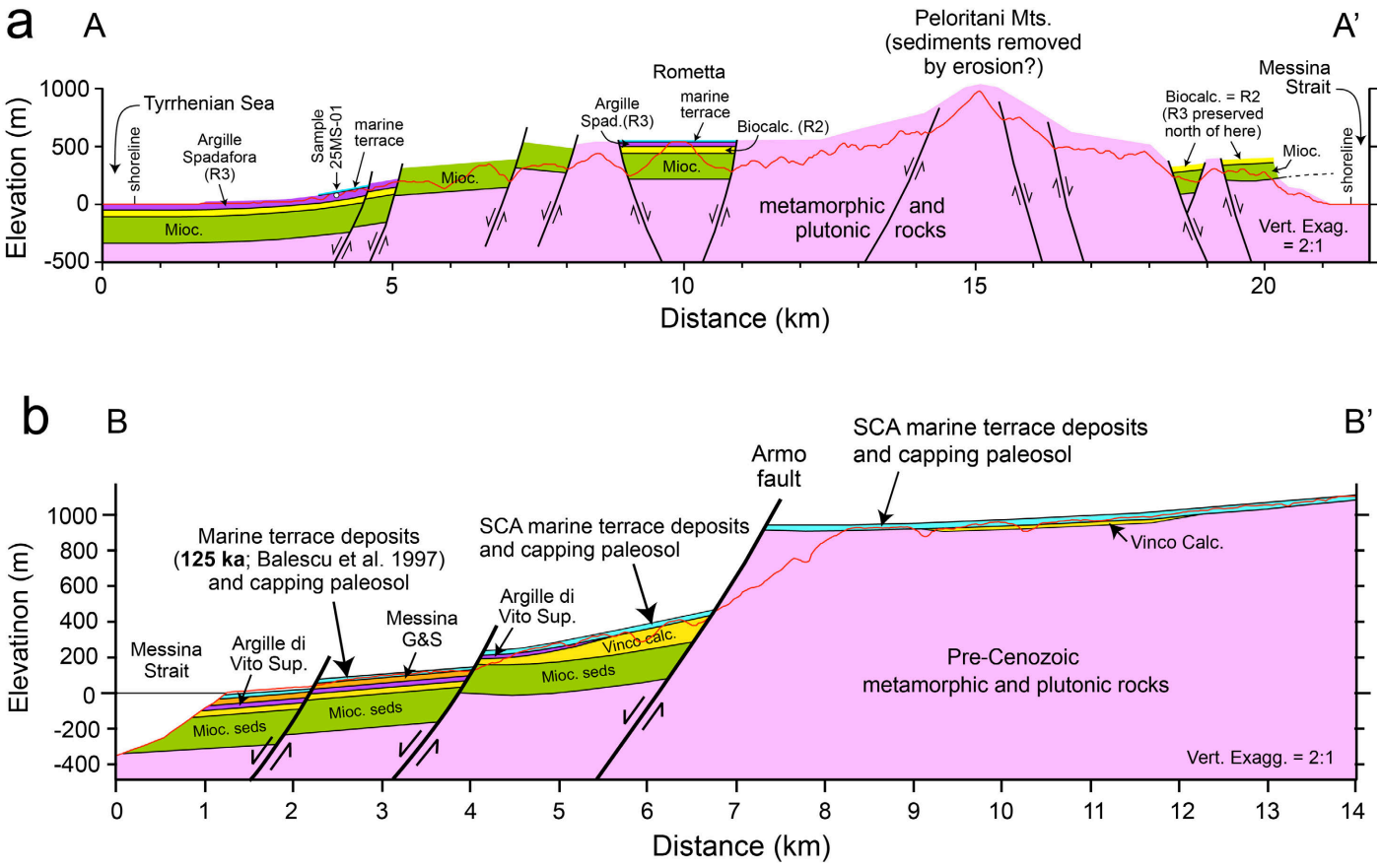

Figure 6. Geologic cross sections across NE Sicily (a) and southern Calabria (b), constructed from map data in Ghisetti et al. (1983), Lentini et al. (2000), Di Stefano et al. (2007). Location shown in Fig. 1. R2 and R3 are units of the Rometta succession (Fig. 4a; Di Stefano et al., 2007).

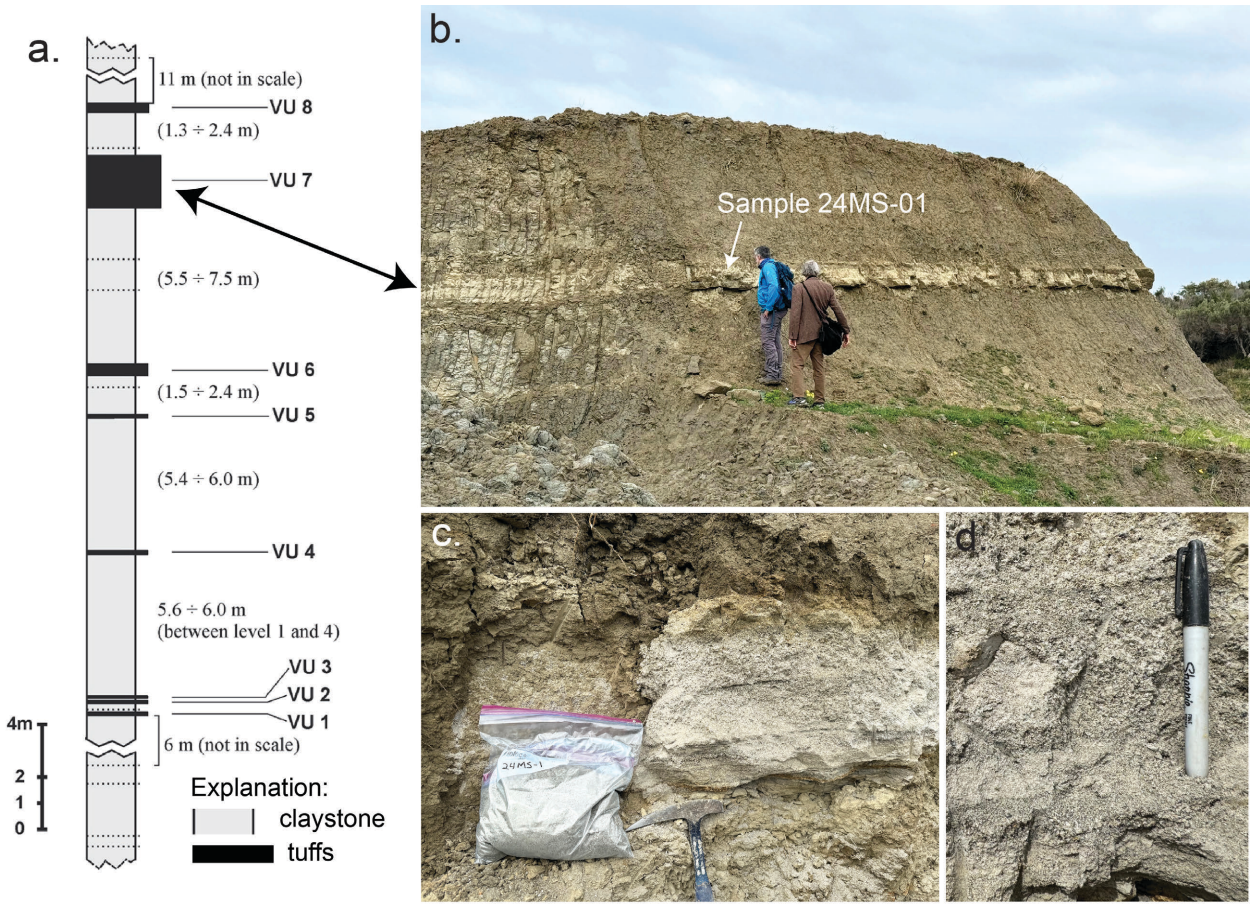

Figure 7. Outcrop photos of tuff interbedded in marine claystone of the Argille di Spadafora (location in Fig. 1). a. Stratigraphic column modified from Di Bella et al. (2016), showing position of volcanic unit VU7. b. Field photo of collection site for Sample 24MS-01 in a recently active clay quarry. c, d. Photos of the sampled tuff showing stratified white lapilli and fresh volcanic glass shards.

4.2 $^{40}Ar/^{39}Ar$ geochronology of the Spadafora Tuff

Sample 24MS-01 is from a laterally extensive ~0.8-m thick volcanic tuff, VU7, in the upper part of Argille di Spadafora (Figs. 4, 6; Di Bella et al., 2016). The tuff contains stratified white lapilli with abundant fresh volcanic glass shards (Figs. 7, 8) and was deposited by a submarine turbidity current from a single volcanic eruption (Di Bella et al., 2016). Dating of tuff 24MS-01 was particularly challenging because of the low K content of plagioclase and high vesicularity of the glass (despite its excellent freshness; Fig. 8), which translate into high atmospheric Ar contents and high analytical uncertainties. A first attempt was completed on a plagioclase separate using the total fusion technique, which yielded for a total of twenty-two grains analyzed individually, ages ranging at face value from ~0.4 to ~0.8 Ma but overlapping within analytical uncertainties, with a weighted-mean age of 0.52 ± 0.11 Ma (Fig. 9a). In a second attempt, both plagioclase and glass separates were

irradiated and analyzed by both the laser total fusion and laser step-heating techniques. Fifteen crystals of plagioclase analyzed individually gave a weighted-mean age of 0.514 ± 0.075 Ma, indistinguishable from the mean obtained in the first irradiation (Fig. 9b). Eighteen total fusion analyses of splits consisting of three grains of the glass shard separates, yielded a similar but more precise mean age due to higher gas yield of 0.517 ± 0.029 Ma (Fig. 9c).

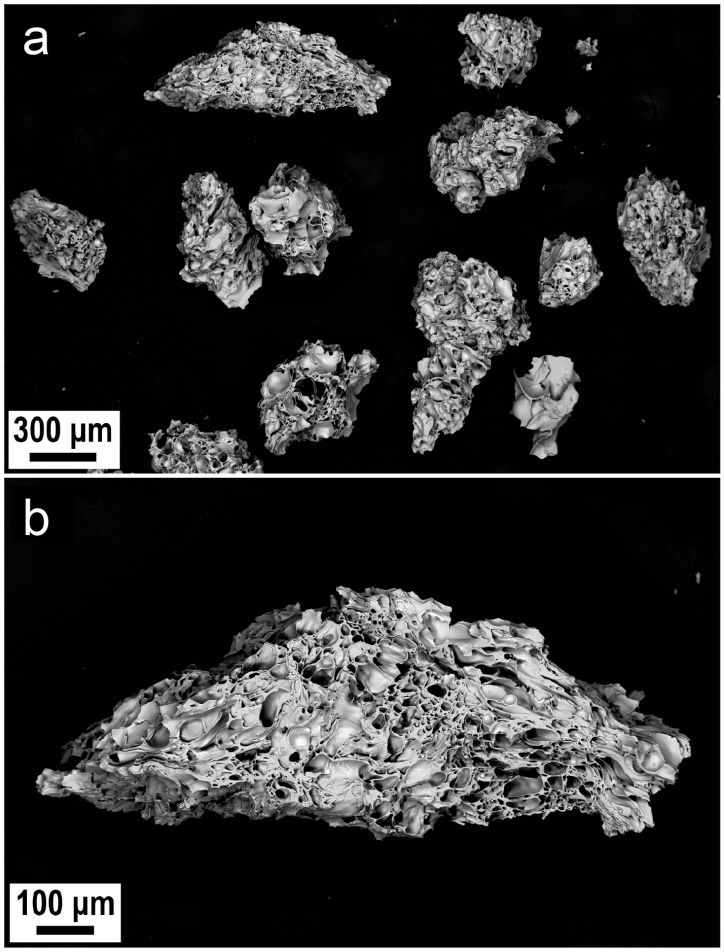

Figure 8. Back-scattered electron images collected by the FE-SEM from the glass separate of tuff 24MS-01 (unit VU7). The separate was analyzed by the laser step-heating technique. Note the excellent freshness and the very high vesicularity of the glass. (a) Several pieces of glass. (b) Closer view of one piece at the top-center of image in a.

Duplicate step-heating runs were completed on both plagioclase and glass multigrain splits (methods described above). Plagioclase yielded concordant heating steps in both runs (Fig. 9d), with weighted mean ages of ~0.46 and ~0.48 Ma, and a pooled mean age of 0.472 ± 0.022 Ma, slightly younger but still within uncertainties (at 2σ level) with age results from total fusion experiments. Unlike plagioclase, the two aliquots of glass shards yielded reproducible discordant age spectra (Fig.

9e), characterized by an initial concordant segment representing ~80–90% of the total $^{39}Ar_K$ released with nearly constant K/Ca ratios (from neutron-produced $^{39}Ar_K$ and $^{37}Ar_{Ca}$ isotopes) and yielding indistinguishable mean ages of 0.480 ± 0.031 and 0.481 ± 0.024 Ma. The concordant segments are followed in the final heating steps by rising ages, up to 0.8–2.5 Ma (Fig. 9e) and lower K/Ca (generally lower than 1), that is suggestive of contamination by an extraneous Ar component (either excess or inherited Ar; Kelley, 2002) most likely hosted in a distinct phase (Di Vincenzo et al., 2025). As a consequence, the total gas ages are slightly to significantly older than the concordant segments (up to ~120 ka older), with the implication that K–Ar dates of glass from the literature (Cornette et al., 1987) most likely represent a maximum age limit for emplacement of the tuffs in the Argille di Spadafora and Argille di Vito Superiore.

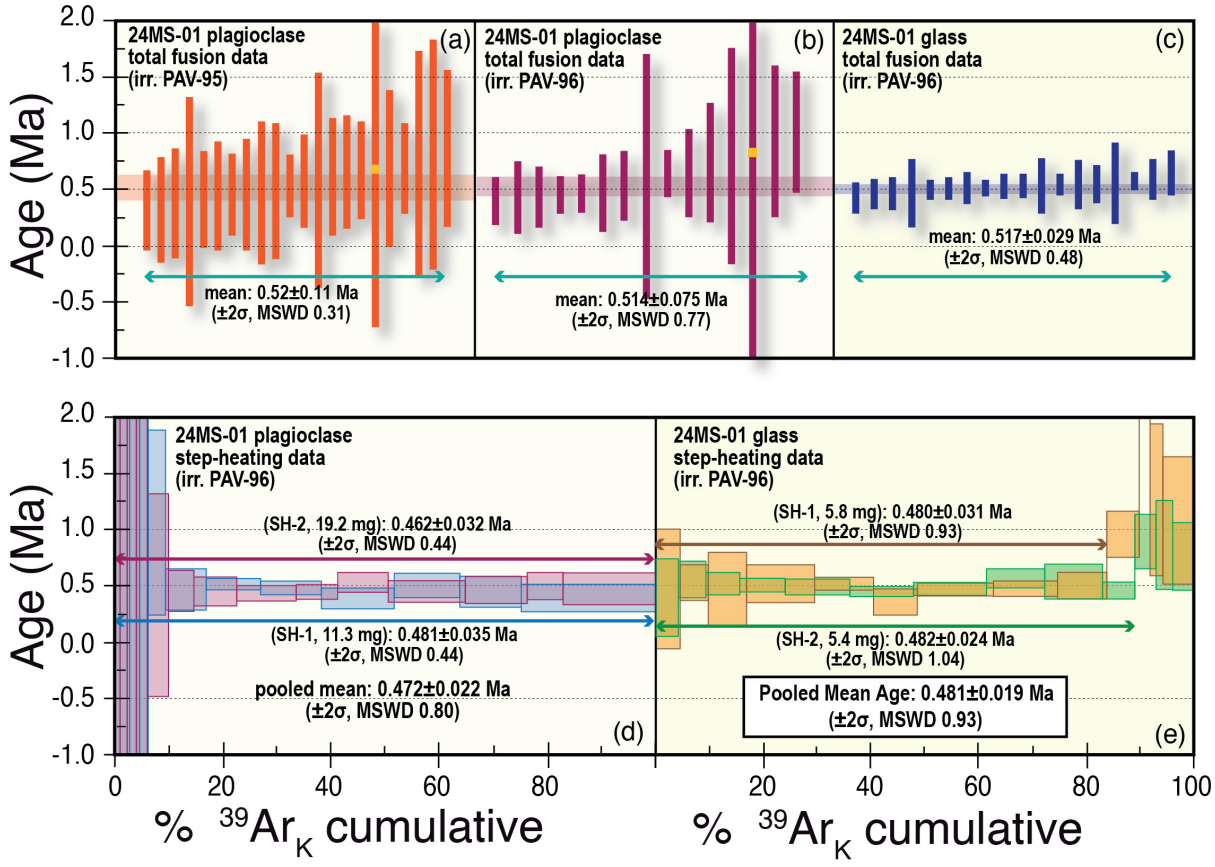

Figure 9. (a-c) Ranked distribution of 40Ar/39Ar ages from total fusion experiments on plagioclase and glass shard separates of tuff 24MS-01 (unit VU7, upper part of Argille di Spadafora – Di Bella et al., 2016). Bars represent 2σ analytical uncertainties. (d-e) Age release spectra of plagioclase (d) and glass (e) separates. Concordant segments in the step-heating experiments on glass (e) yield a pooled mean age of 0.481 ± 0.019 Ma (481 ± 19 ka) (±2σ). Box heights indicate the 2σ analytical uncertainty. Errors on weighted-mean ages are 2σ internal uncertainties. MSWD indicates the mean square of weighted deviates.

In light of the higher K contents of the glass, which translate into higher gas yield and lower analytical uncertainties, and the higher resolving power of the step-heating technique, the concordant segments from step-heating experiments on glass are considered to yield the most reliable estimate for the time of emplacement of tuff 24MS-01. The pooled mean age of 481 ± 19 ka (±2σ) corresponds to the youngest part of subzone MNQ19d (960–460 ka; Di Stefano et al., 2023), which has recently replaced biozone MNN19f with a previously reported age range of 990–580 ka (Di Stefano et al., 2007; Di Stefano & Lentini, 1995; Di Stefano & Longhitano, 2009; Lentini et al., 2000; Pino, Baldanza, et al., 2007; Pino, Belfiore, et al., 2007).

4.3 Correlation of the Spadafora Tuff to Southern Calabria

Prior studies show that the Argille di Spadafora in NE Sicily correlates to bathyal marine clays and marls of the Argille di Vito Superiore in southern Calabria (Figs. 4, 6; Carbone et al., 2022; Di Geronimo et al., 1997; Di Stefano et al., 2007; Ghisetti et al., 1983; Jacques et al., 2001; Lentini et al., 2000) whose age ranges from ~ 1.0 to 0.5 Ma based on paleomagnetism of clays and K-Ar ages of interbedded tuffs (Aïfa et al., 1988; Cornette et al., 1987). Deep marine clays and marls in both areas conformably overlie shallow marine bio-calcarenites and record a period of accelerated subsidence, deepening, and transgression. Based on similar lithology, stratigraphic position, age, and limited thickness, we conclude that the marine clays and marls correlate in time with little or no diachronism across the Messina Strait (Carbone, et al., 2022). We tried to test this correlation by dating tuffs reported from southern Calabria (Cornette et al., 1987; De Rosa et al., 2008; Jacques et al., 2001), but the tuff beds were not accessible due to recent residential development, agriculture, or cover. The claystone-marl unit is overlain by two younger units: (1) MGS gravels and sands; and (2) capping Pleistocene marine terrace deposits (Fig. 4). The regional stratigraphic correlation, $^{40}Ar/^{39}Ar$ age of the Spadafora tuff (481 ± 19 ka), and recognition that an unknown amount of time is represented by the MGS deposits, all indicate that the capping marine terraces are younger than 0.50 Ma.

4.4 Paleoshoreline Modeling of Marine Terraces

We performed paleoshoreline modeling of marine terraces at Campo Piale (Fig. 10; Table 1, 2) using the synchronous correlation method described above. A widespread surface preserved at ~125–190 m asl from Arghillà district to Piale is assigned to the last interglacial highstand at 125 ka (MIS 5e). This terrace is displaced ~100 m down to an elevation of 80–90 m asl in the hanging wall of

a strand of the Scilla fault in the Cannitello area (Monaco et al., 2017). Assuming the Campo Piale profile follows an intact un-faulted ridge between faulted areas to the north and south (Fig. 10), we assign higher-elevation terraces to successively older sea-level highstands following the precedent of previous studies (Antonioli et al., 2021; Dumas et al., 2000, 2005; Meschis et al., 2022; Miyauchi, 1994; Monaco et al., 2017). Higher-elevation surfaces are more deeply incised and less continuous, except for the 600–630 m surface in the Piani di Melia (Fig. 10). Distinct terrace levels and assigned sea-level highstands include: MIS 5e (125 ka) at 195 m asl; MIS 7e (240 ka) at 280 m asl; MIS 9c (310 ka) at 330 m asl; and MIS 9e (340 ka) at 406 m asl (Fig. 10). Less well-defined terraces are picked at 520 m asl (MIS 13a; 478 ka) and 590 m asl (MIS 13c; 525 ka) (Fig. 10; Table 2). The highest widespread surface at the top of the Campo Piale profile is the Piani di Melia, in the footwall of the Scilla fault (Figs. 1, 2), to which we assign an age of <590 ka (MIS 15e) (Fig. 10; Table 2). This age falls within the range of previous estimates (Miyauchi, 1994; Monaco et al., 2017; Antonioli et al., 2021), thus replicating the results of prior studies. Figure 11 shows strong correlation between predicted and observed terrace elevations. The results of our shoreline modeling imply that the uplift rate in this area accelerated from 0.97 mm/y before 50 ka to 2.2 mm/y after 50 ka, similar to results of previous investigations (Antonioli et al., 2021; Meschis et al., 2022).

In summary, paleoshoreline modeling suggests an age of ~525–590 ka for the high marine terrace in the footwall of the Scilla fault at 600–630 m elevation (Figs. 10, 11; Table 2). This is an overestimate because it assumes no fault offsets, tilting or fault-related warping, despite abundant evidence for these processes in the study area. Difficulty of correlating the highest surface in the profile to a unique sea-level highstand produces added uncertainty. We therefore infer an age of ~500–600 ka for the 630-m terrace, which implies a time-averaged uplift rate of ~1 mm/y for the Piani di Melia terrace in the footwall of the Scilla fault.

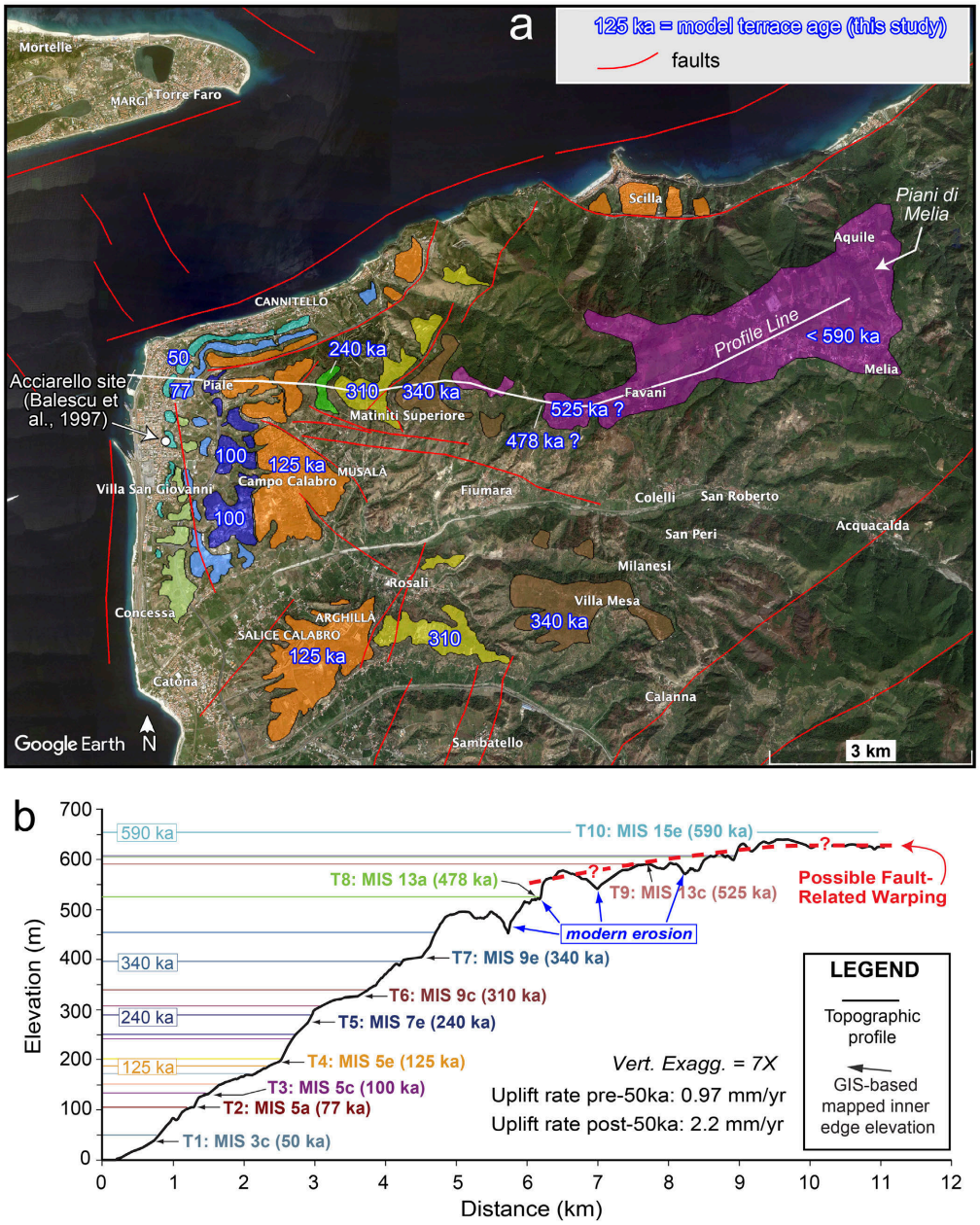

Figure 10. (a) Map of uplifted marine terraces and inferred ages on Campo Piale ridge (location in Fig. 1). Terraces at and below 200 m elevation are known from prior studies (e.g., Balescu et al., 1997; Dumas et al., 2005; Antonioli et al., 2021). Terrace ages above 200 m are derived from shoreline modeling (this study). (b) Topographic profile extracted from 10-m DEM in QGIS (profile line in A). Inflections in the profile (T1 - T10) represent "measured" palaeoshorelines assigned to marine isotope stages (MIS) and corresponding sea-level highstands based on shoreline modeling. Modern erosional valleys at higher elevations add some uncertainty to shoreline picks. Horizontal lines are "predicted" shoreline elevations derived from an uplift model that minimizes the misfit between measured and predicted elevations (Fig. 11). Shoreline picks in this model assume no faults, tilting, or warping, so that each higher surface records a successively older global sea-level highstand. Under these assumptions, the 630-m surface is bracketed between 525 and 590 ka. Introduction of fault offsets, tilting, or fault-related warping (red dashed line) would imply a younger age for the 630-m surface.

Table 1. Ages and heights of global marine highstands used in this study.

Age (ka) *	Marine Isotope Stage (MIS)	Height of Highstand (m)
0	1	0
30	2	-80
50	3c	-60
76.5/80	5a	-30
100	5c	-25
115	5	-21
119	5	-5
125	5e	5
175	6	-30
200	6	-5
217	6	-30
240	7e	-5
285	8	-30
310	9c	-22
340	9e	5
410	11	-5
478	13a	0
525	13c	20
550	14	10
560	14	3
590	15e	20
620	16	20
695	17	10
740	18	5
800	19	20
855	21	20

* Sea level ages and highstands from Rohling et al. (2014) and Siddall et al. (2003)

Table 2. Mapped inner edges and proposed refined ages.

Terrace Name	UTM Coordinate (Easting)	UTM Coordinate (Northing)	Measured Elevation (m)	Predicted Elevation (m)	Proposed Age (ka)	Marine Isotope Stage (MIS)
T1	0556082	4231183	40	50	50	3c
T2	0556285	4231713	105	106	77	5a
T3	0556690	4231154	130	134	100	5c
T4	0557894	4231107	195	188	125	5e
T5	0558301	4231073	280	289	240	7e
T6	0559206	4231041	330	340	310	9c
T7	0559928	4231158	406	396	340	9e
T8	0561063	4231156	520	525	478	13a
T9	0561704	4230991	590	591	525	13c
T10	0566007	4232440	630	654	590	15e

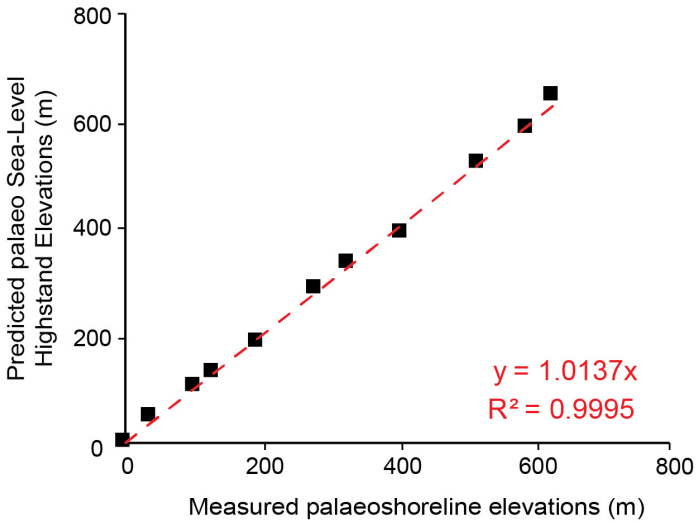

Figure 11. Plot of predicted palaeoshoreline elevations versus measured shoreline elevations (see Fig. 10), assuming uplift rates of 0.97 mm/y prior to 50 ka and 2.2 mm/y from 50 ka to the present. The model uplift history minimizes the misfit between measured and predicted palaeoshoreline elevations. The margin of uncertainty for measured and predicted elevations is ≤ the size of symbols. See text for details.

4.5 Fault Zone Morphology

Compilation of regional faults and geomorphology shows that uplifted marine terraces in southern Calabria are cut and offset by active normal faults across a wide range of elevations and displacement magnitudes (Figs. 1, 2; Aloisi et al., 2013; Catalano et al., 2008; Meschis et al., 2022; Roda-Boluda and Whittaker, 2017). The fault network displays many features characteristic of active normal fault systems, including triangular facets and wineglass canyons (Catalano et al., 2008; Ferranti et al., 2007; Tortorici et al., 1995), a large conjugate relay zone that forms the narrow passage of the Messina Strait (Dorsey et al., 2024); curved faults with pronounced slip gradients from fault center to tip; NW-striking transfer faults that connect NE-striking normal faults (e.g., faults that link the Calanna and Armo faults); a complex group of NNE-striking short fault segments in the 2-km wide Reggio Calabria fault zone; and a prominent relay ramp that accommodates transfer of strain from the Cittanova to the Sant'Eufemia fault (Fig. 1).

A 3D oblique view looking southwest at the slope map reveals deep incision into the relay ramp and a decrease in elevation of the SCA terrace down the ramp between the two bounding normal faults (Fig. 12a). The dipping terrace correlates across a 250–300 m deep canyon as it descends from 850–1100 m at the top of the ramp to 500–600 m at the bottom (Fig. 12b). A cross-strike profile shows minimal offset of the SCA terrace across the Cittanova fault near its southwest termination, gentle NW dip down the broad Piani d'Aspromonte from ~1200 to 1000 m elevation,

and ~400 m offset across two strands of the Sant'Eufemia fault which drops the SCA terrace down to ~500–600 m elevation in the footwall of the Scilla fault (Fig. 12c).

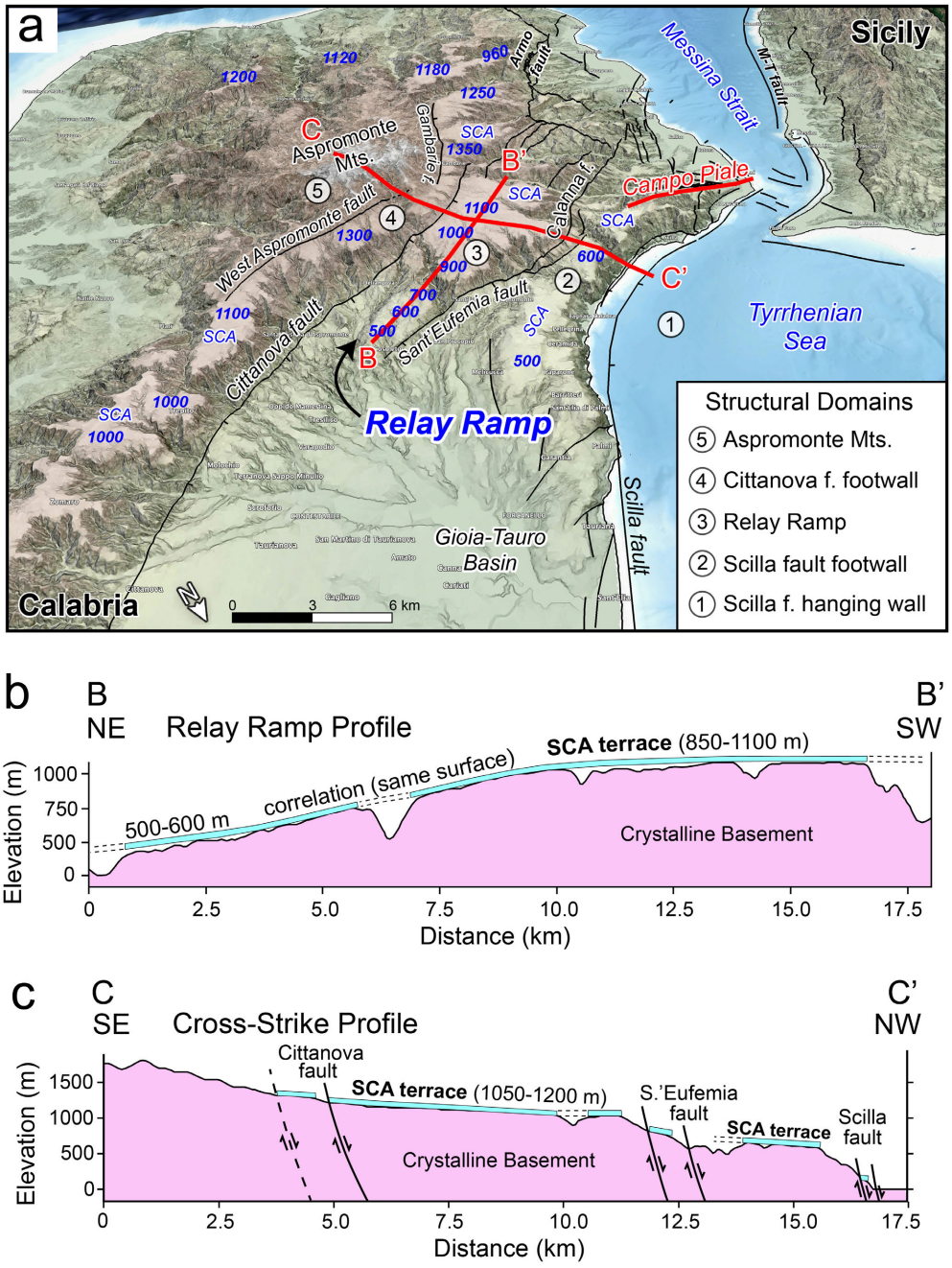

Figure 12 (a) Oblique view looking southwest at normal faults and marine terraces on slope map extracted from 10-m DEM (Fig. 2b). SCA is the SCA marine terrace at a wide range of elevations (labeled with blue numbers). A large relay ramp transfers extensional strain from the Cittanova fault in the north to the Sant'Eufemia fault in the south. (b) Along-strike topographic profile (B-B') down the relay ramp shows gradual decrease in elevation from >1 km to 500-600 m, and correlation of the SCA marine terrace down the ramp. (c) Cross-strike topographic profile (C-C') showing fault offset of the SCA terrace which correlates across the Sant'Eufemia fault (parts a, b).

A closer view of the relay ramp (Fig. 13) reveals evidence for active fault growth, fault-tip propagation, and transfer of strain between the Cittanova and Sant'Eufemia faults. The inclined terrace surface climbs from ~500 m asl at the bottom of the ramp to >1,000 m at the top, and from there it is displaced across the Sant'Eufemia and Calanna faults from the high Piani di Aspromonte down to the Piani di Melia terrace at 500-600 m elevation. The Piani di Aspromonte is incised by deep canyons arranged in a quasi-radial pattern emanating from the Aspromonte Mountains in the footwall of the Western Aspromonte and Gambarie faults. Two modern channels are deflected around the NE tip of the Sant'Eufemia fault, revealing the dynamic surface response to active NE propagation of the Sant'Eufemia fault (Fig. 13).

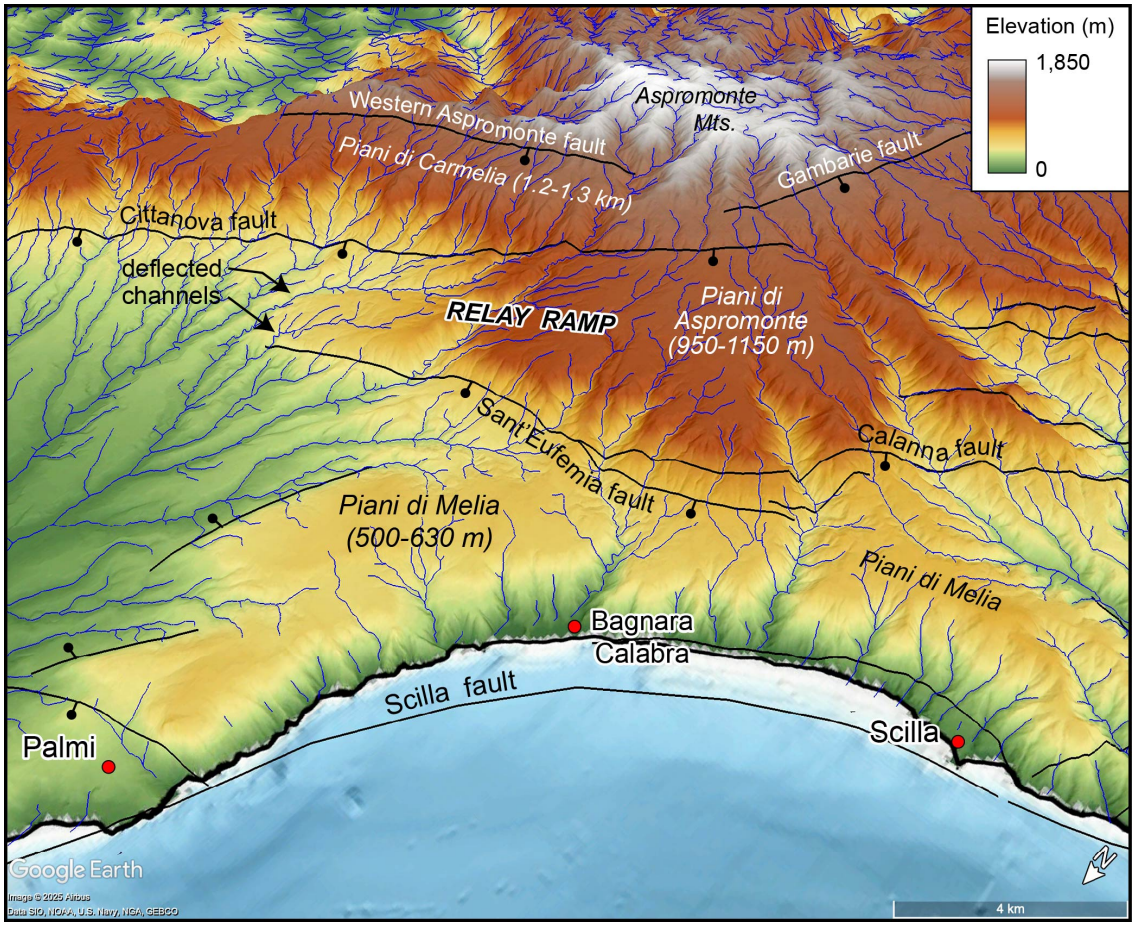

Figure 13. Oblique 3D view looking southeast at 10-m color DEM highlighting the relay ramp, which transfers extensional strain between the Cittanova and Calanna-Sant'Eufemia faults. Note modern channels deflected around the NE tip of the Sant'Eufemia fault at the lower end of the ramp, indicating active landscape response to fault propagation and growth of the relay ramp.

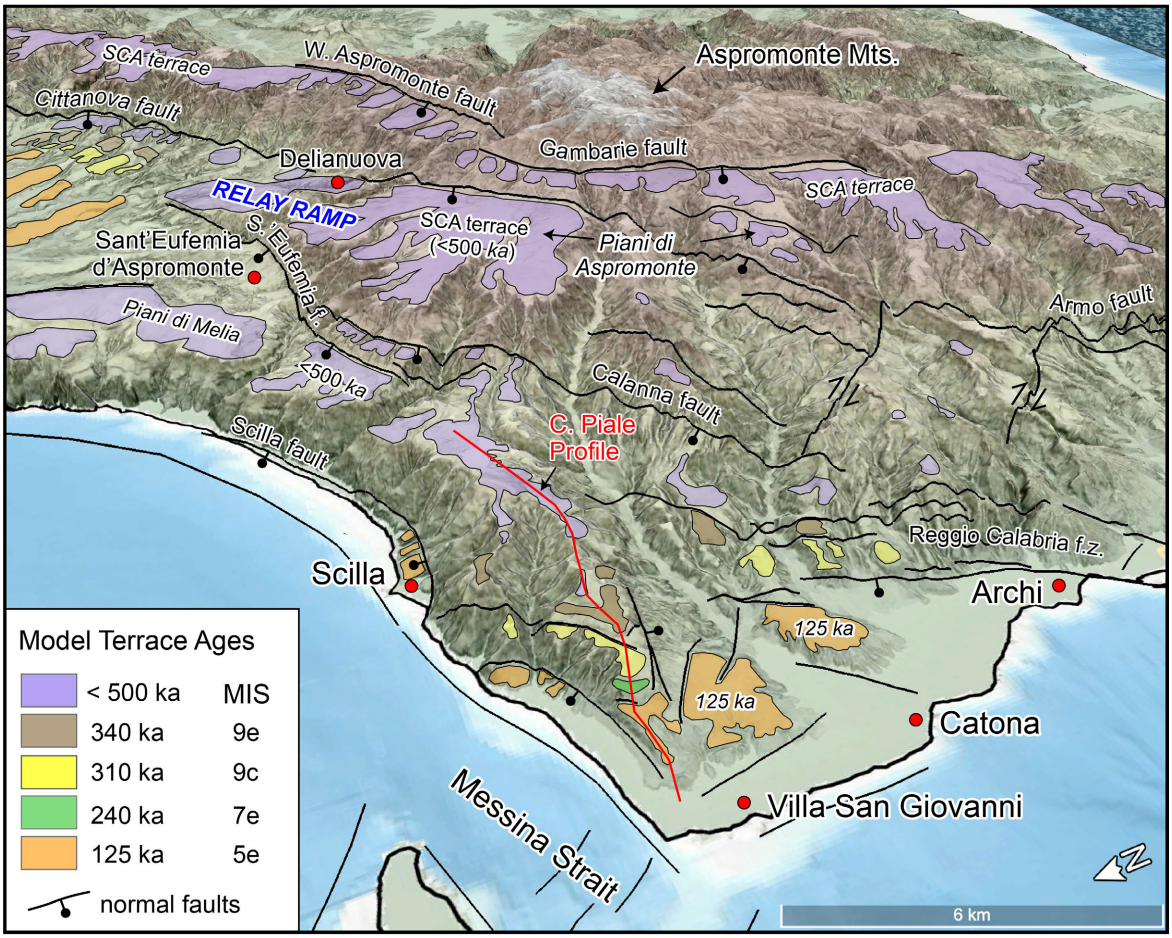

Figure 14. Oblique 3D view looking ~ east at the geomorphic expression of normal fault network in southern Calabria (plotted on slope map from 10-m DEM, overlaid in Google Earth) with uplifted marine terraces colored by interpretation of this study (Figs. 10, 11). Presence of a large relay ramp, and seismically active faults separating terrace remnants at different elevations, indicate that the terrace at 500-600 m elevation (Piani di Melia) correlates to the high SCA terrace at elevations up to 1.2-1.3 km asl (Piani di Aspromonte). MIS is marine isotope stage.

Figure 14 shows more diagnostic fault features including a steep 500-600 m high scarp in the footwall of the Scilla fault, common triangular facets and intervening wineglass canyons in footwalls of the Scilla, Sant'Eufemia and Cittanova faults, abrupt downstream decreases in erosional relief across active normal faults, and numerous remnants of the structurally dismembered and incised SCA terrace. In summary, diagnostic fault geometries (Figs. 12–14), geochronologic and stratigraphic data (Figs. 4, 9), and paleoshoreline modeling of marine terraces (Figs. 10, 11), all support an interpretation that marine terrace remnants in the Piani di Melia and Piani di Aspromonte represent a once-contiguous geomorphic surface that has been offset, uplifted, tilted and eroded in the past ~500 ky (as noted by Catalano et al., 2008). Previous studies established that the Argille di Spadafora in NE

Sicily correlates to similar clays and marls of the Argille di Vito Superiore in southern Calabria (Fig. 4; Carbone et al., 2022; Cornette et al., 1987; De Rosa et al., 2008; Di Geronimo et al., 1997; Ghisetti, 1981; Jacques et al., 2001). Applying these constraints, we conclude that all Pleistocene terraces up to 1.3 km asl in a large area between the Aspromonte Mountains and Messina Strait coastline (Fig. 1) are younger than the Argille di Spadafora and Argille di Vito Superiore, and therefore are < 0.50 Ma.

5. DISCUSSION

5.1 Age of the SCA Marine Terrace

The $^{40}Ar/^{39}Ar$ age of the Spadafora tuff (0.481 ± 0.019 Ma) is the first modern isotopic age determination for Pleistocene tuffs in NE Sicily and is consistent with existing biostratigraphy for the Argille di Spadafora, falling at the young end of nannoplankton subzone MNQ19d (960–460 ka; Di Stefano et al., 2023). The Argille di Spadafora correlates stratigraphically and in time with Argille di Vito Superiore in Calabria, which ranges from ~ 1.0 to 0.5 Ma and is unconformably overlain by MGS gravels and capping marine terrace sediments (Fig. 4). When integrated with regional stratigraphy and fault-zone morphology, our results indicate an age of < 500 ka for the high SCA marine terrace at 1.0–1.3 km asl (Piani di Aspromonte) in the footwall of the Cittanova, Sant'Eufemia and Armo faults (Fig. 14). This age is consistent with prior estimates for the Piani di Melia at ~ 500–600 m asl (Catalano et al., 2008; Monaco et al., 2017) and is roughly half the widely cited age of 1.0 ± 0.2 Ma for the high SCA terrace (Miyauchi, 1994; Roda-Boluda & Whittaker, 2017). Because this revised age is important for constraining crustal uplift and fault slip rates, we explore it in more detail below.

Previous age estimates for the high SCA terrace were based on: (1) presence of cool-water foraminifers *Globorotalia truncatulinoides excelsa* and *Hyalinea balthica,* and the mollusk *Arctica islandica*, which are often called "northern guests" because they first appeared in the Mediterranean region during onset of northern hemisphere glaciation at ca. 1.8 Ma (Barrier et al., 1986; Crippa et al., 2016; Miyauchi, 1994); (2) K–Ar age of ~0.72 Ma from a tuff in Argille di Vito Superiore which is older than the terrace deposits (Fig. 15a) (Cornette et al., 1987); and (3) paleoshoreline models that assume sea-level changes superposed on an intact, un-faulted uplifting region (e.g., Dumas et al., 2000, 2005; Miyauchi, 1994). Barrier et al. (1986) stated that the presence of cool-water species in the terrace deposits means the sediment accumulated *at the time of* faunal first appearances in the region. However, this claim must be rejected because the species are all extant (alive today), which means the deposit could have formed any time *after ca. 1.8 Ma*. Miyauchi (1994) adopted the age

assignment of Barrier et al. (1986) and used it to construct a detailed chronology that assumed higher terraces are older, concluding that the high SCA terrace is ca. 1.0 – 1.2 Ma. This age model has become widely accepted in the modern literature without challenging the flawed logic of the original age determination. Age assignments based on paleoshoreline models are subject to uncertainties that arise from a common but unstated assumption that the terraces are not offset by faults (Fig. 3). A recently obtained maximum depositional age of 750–900 ka for the SCA terrace based on $^{40}Ar/^{39}Ar$ dating of detrital sanidine (Perez et al., 2024) represents an upper age limit consistent with our result. In summary, all attempts to date the SCA marine terrace using direct age constraints, including this study, rely on methods that yield a maximum upper age limit, not a true depositional age. While it is often tempting to interpret maximum depositional ages as true depositional ages, this inference is not credible without independent corroborating data which currently are lacking.

Figure 15a shows the simplified stratigraphy of southern Calabria compiled from prior studies (Ghisetti et al., 1983; Barrier, 1987; Jacques et al., 2001), as shown to scale in the geologic cross section (Fig. 6b). Paleomagnetism, biostratigraphy, K-Ar tuff ages, and correlation to the Spadafora tuff (this study) show that Argille di Vito Superiore ranges in age from ~ 1.0 Ma at the base where it gradationally overlies Vinco Calcarenite, to ~ 0.5 Ma at the top where it is unconformably truncated at the sharp base of MGS (Fig. 4b; Aïfa et al., 1987, 1988; Barrier, 1987; Cornette et al., 1987). Because Argille di Vito Superiore is not preserved beneath the high SCA terrace in the east, the age of terrace sediments is not directly constrained in that area, suggesting they could be older. However, an age of ca. 1 Ma for the high SCA terrace (e.g., Miyauchi, 1994) would require that these deposits correlate to the 1.0-Ma base of Argille di Vito Superiore in the central and western blocks, an idea that is not supported by observed stratigraphic relationships (Fig. 15a). Two previous studies correlated the SCA terrace across the Armo fault in southern Calabria (Roda-Boluda and Whittaker, 2017; Quye-Sawyer et al., 2021), and we concur with this interpretation. Correlation of the terrace deposits is supported by: (1) recognition of an active relay ramp and tracing of the terrace up the ramp from ~ 600 m to > 1.0 km elevation (Figs. 12 – 14); (2) stratigraphic superposition that shows the terrace sediments are everywhere younger than Vinco Calcarenite and Argille di Vito Superiore (Fig. 15a); (3) absence of uncemented fossiliferous sands in older sedimentary units; and (4) striking similarity of uncemented shallow marine sands and beach deposits capped by thin immature red soils (inceptisols) in terrace sediments across a wide range of elevations (Fig. 5). The hypothesis for older terraces at higher elevations predicts longer duration of subaerial exposure that should produce deeper, more mature

soils at the highest elevations. Our field observations and other studies instead reveal a similar weak degree of soil development across the full range of elevations in the study area (Costantini & Dazzi, 2013; Rivieccio, 2020), further supporting the terrace correlation.

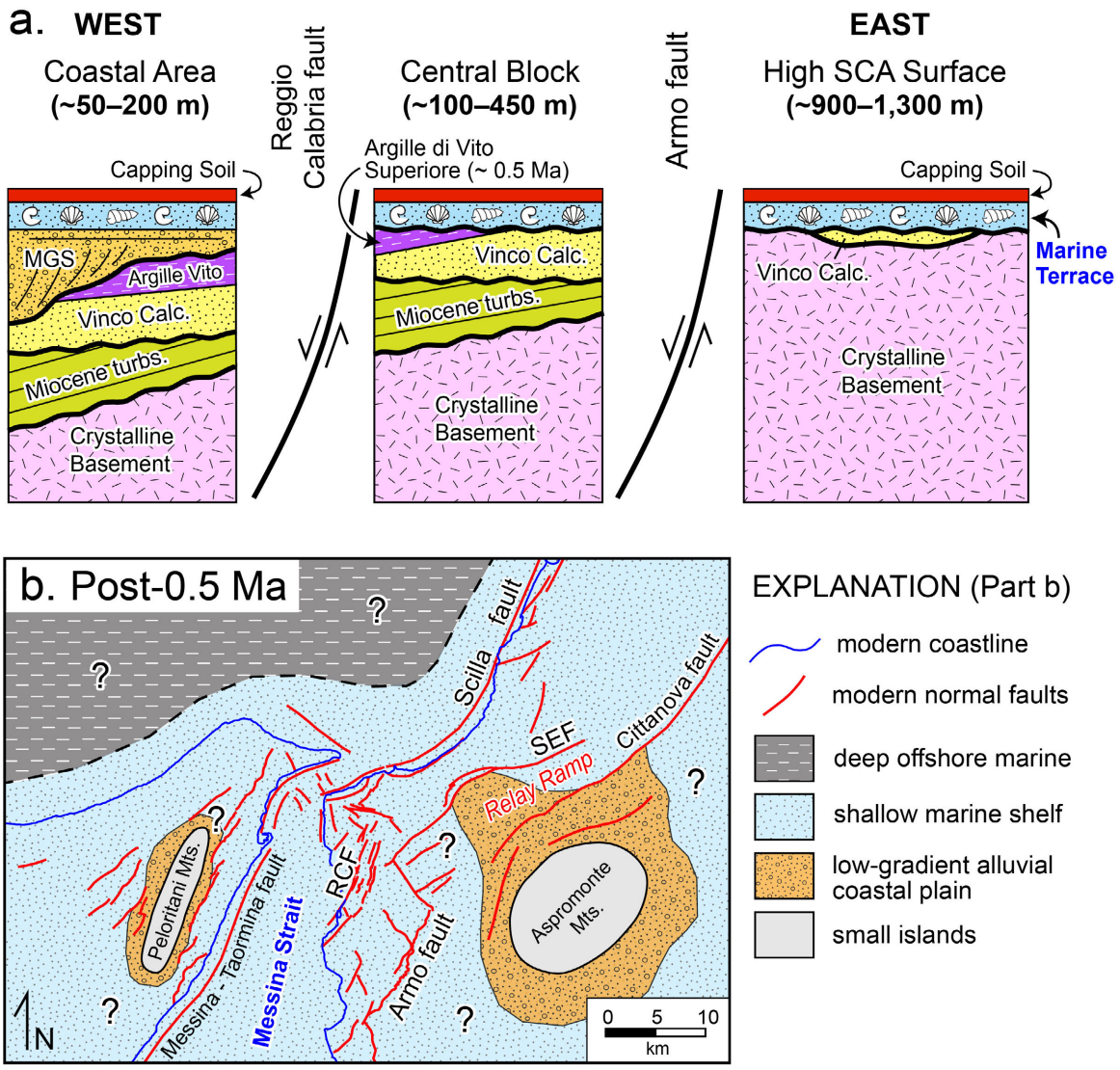

Figure 15. a. Simplified stratigraphy of Cenozoic deposits in SW Calabria, east of Messina Strait (Fig. 1). Numbers in parentheses are the range of elevation for marine terrace deposits in each fault domain (Fig. 2a). Terrace sediments rest on an unconformity in the eastern and central blocks (footwall of Armo and Reggio Calabria faults), and they conformably overlie MGS in the western coastal area (expanded section). b. Proposed paleogeographic reconstruction for Pleistocene marine terrace deposits, after 0.5 Ma and prior to onset of differential uplift on modern normal faults. Terrace sediments accumulated in a wide shallow marine shelf with small isolated islands flanked by low-gradient coastal plains, and later were uplifted and dissected by modern normal faults.

Other hypotheses for an older age of the high SCA marine terrace are similarly inconsistent with data and observations. In one idea, Argille di Vito Superiore may have accumulated at bathyal water depths in hanging-wall basins adjacent to syn-depositional normal faults, while coeval SCA terrace deposits formed in a shallow marine shelf on nearby footwall uplifts. This is potentially supported by stratigraphic evidence for faulting during deposition of the Vinco Calcarenite (e.g., Barrier, 1986; Chiarella et al., 2021), and map relations that show Pleistocene deposits thicken into hanging-wall blocks and thin onto footwall uplifts (Figs. 1, 6b; Ghisetti et al., 1983). However, this hypothesis predicts lateral thickening and coarsening of the clay-marl unit into conglomeratic base-of-scarp facies near normal faults, yet these relationships are not observed. Instead, the uniformly fine-grained Argille di Vito Superiore is eroded and truncated by an angular unconformity at the base of the younger terrace unit (Fig. 15a). The regional claystone-marl unit and older calcarenites may be time-transgressive with ages changing laterally across the Messina Strait, but this model predicts shoreline migration toward paleo-topography in the Aspromonte Mountains which would make clay and marl in Calabria younger, not older, than the Spadafora tuff in NE Sicily. In short, the marine terrace sediments cannot be older than 0.5 Ma because they overlie and are younger than Argille di Spadafora, Argille di Vito Superiore, and MGS everywhere in the study area (Figs. 4, 6b, 15a).

Building on the above analysis, we propose a paleogeographic reconstruction that restores the SCA marine terrace sediments to their depositional position, sometime after 0.5 Ma and prior to the onset of differential uplift on modern normal faults (Fig. 15b). Sediments accumulated in a wide shallow marine shelf with small, isolated islands (future Aspromonte and Peloritani mts.) that were flanked by low-gradient fluvial coastal plains (e.g., Quye-Sawyer et al., 2021). Other known examples of Pleistocene extension-related uplift and inversion of a former marine shelf include: (1) northern Peloponnese, south of the modern Gulf of Corinth, in response to normal fault migration and rift localization (Armijo et al., 1996; de Gelder et al., 2019; Fernández-Blanco et al., 2019; Ford et al., 2017); (2) Kythira Island in the Hellenic arc where uplift may be driven by propagation of the North Anatolian Fault, incipient collision with the African plate, or mantle dynamics (de Gelder et al., 2022; Gaki-Papanastassiou et al., 2011; van Hinsbergen et al., 2006; Veliz-Borel et al., 2022); and (3) the southern Anatolian plateau where uplift and extension are driven by asthenospheric upwelling through tears and breaks in the subducting Aegean slab (Aykut et al., 2025; Öğretmen et al., 2018; Racano et al., 2021; Schildgen et al., 2012).

5.2 Regional Tectonic Implications

The young age of the Spadafora tuff has important implications for understanding the Pleistocene tectonic development of NE Sicily and southern Calabria. With a paleo-water depth of 500–700 m, presence of Argille di Spadafora at 500 m elevation in Rometta (Fig. 6a) means the crust there has been uplifted ~ 1000–1200 m in the past 0.50 My, suggesting an average rate of ≥ 2 mm/y. This represents a minimum estimate for adjacent areas because the Rometta succession is down-dropped ~ 300 m in a normal fault-bounded graben (Fig. 6a), so post-500 ka rock uplift southeast of there is greater by at least 300 m. If a Cenozoic sedimentary section similar to the Rometta succession was eroded off the crest of the Peloritani Mountains (1,000 m asl; Fig. 6a), the Argille di Spadafora would restore to ~ 1,300 m elevation at the crest of the range and the eroded sediments would likely be recycled and stored in adjacent modern basins of the Messina Strait and Tyrrhenian Sea (Fig. 1). In this case, the implied rock uplift would be ~ 1800–2000 m in the past 500 ky for an uplift rate of ~4.0 ± 0.2 mm/y at the crest of the Peloritani Mts. (Fig. 1). This is faster than uplift rates of 1–2 mm/y based on elevations and ages of marine terraces (Catalano & De Guidi, 2003; De Guidi et al., 2003) and constraints from a study of MGS deposits near the Messina Strait coast in NE Sicily (Pavano et al., 2024), and needs to be tested in future work.

Our analysis of fault-controlled stratigraphic architecture (Fig. 15a), integrated with prior studies (Ghisetti et al., 1983; Barrier, 1986; Jacques et al., 2001; Chiarella et al., 2021), suggests multiple phases of normal faulting in southern Calabria. A complex deformation history is supported by the observation that the base of the marine terrace unit changes laterally from an unconformity in the eastern and central footwall blocks where it rests on basement rock, Vinco Calcarenite and Argille di Vito Superiore, to a conformable contact in the western coastal area where terrace sediments overlie MGS in an expanded section produced by hanging-wall subsidence (Fig. 15a). The first phase of faulting initiated during deposition of the Vinco Calcarenite and produced distinctive base-of-scarp facies and fanning-dip sections that record fault-related tilting during deposition (e.g., Chiarella et al., 2021). We infer that a combination of footwall erosion, hanging wall deposition, and slow fault-slip rates may have generated subdued topographic relief across the Armo fault during this phase. The area was then submerged by increased subsidence, relative sea-level rise, and a change to bathyal conditions recorded in Argille di Vito Superiore (1.0 – 0.5 Ma). Later, renewed slip on the same family of faults drove rapid delta progradation, base-level fall, erosional stripping of footwall uplifts, and deposition of Messina Gravels and Sands (MGS). Fault slip resumed or continued after

deposition of post-0.5 Ma sediments, progressively isolating terrace remnants by fault displacements, footwall uplift, and erosion that continues to the present day (Fig. 1).

Applying our new age constraint yields an average uplift rate of > 2.5 mm/y in the past ~500 ky for the high SCA marine terrace at ~1.2 km asl, which is similar to our post-50 ka rate for the Campo Piale transect (2.2 mm/y; Figs. 10, 11) and maximum post-125 ka uplift rates determined for the Capo Vaticano Peninsula (~1.8–2.0 mm/y; Bianca et al., 2011; Roberts et al., 2013). The terrace surface is displaced by up to ~500 m on the Cittanova and Armo faults (Fig. 2) (Roda-Boluda & Whittaker, 2017), implying variable throw rates up to ca. 1 mm/y. These are minimum rates because the SCA terrace unconformably overlies and is younger than the 0.5-Ma Argille di Vito Superiore (Fig. 15a). Uplift in Calabria is widely considered to be driven by toroidal flow of the upper mantle into migrating tears in the Ionian slab (e.g., Clementucci et al., 2024; Faccenna et al., 2011, 2014; Gallen et al., 2023). Our results are consistent with this model and suggest that the surface response to mantle processes may be faster than commonly inferred.

Based on joint inversion of bedrock thermochronology, ^{10}Be-derived erosion rates, river channel modeling, and prior studies of marine terraces, Gallen et al. (2023) concluded that rock uplift rates in southern Calabria were slow (<0.4 mm/y) from ~ 15 to 2 Ma, and increased at 1.5–1.0 Ma to current rates of ~ 0.5–1 mm/y. Data presented above suggest an alternative history in which the forearc region of southern Calabria and NE Sicily was undergoing accelerated *subsidence*, not uplift, between 1.0 and 0.5 Ma. This period of regional subsidence and deepening is recorded in well dated bathyal marine claystone (Argille di Spadafora and Argille di Vito Superiore) that conformably overlie shallow marine calcarenites in most areas where Miocene-Pleistocene sediments are preserved (Figs. 1, 4). The claystone-marl unit is documented throughout southern Calabria and NE Sicily with geologic mapping (Carbone et al., 2022; Ghisetti et al., 1983; Lentini et al., (Barrier, 1986; Barrier et al., 1987; Di Stefano et al., 2007; Di Stefano & Longhitano, 2009; Jacques et al., 2001; Longhitano et al., 2012; Messina et al., 2009), biostratigraphy (Di Stefano et al., 2007, 2023; Di Stefano & Lentini, 1995; Lentini et al., 2000; Pino, Baldanza, et al., 2007; Pino, Belfiore, et al., 2007), and paleobathymetric study (Di Geronimo et al., 1997; Girone, 2003; Di Stefano et al., 2007; Violanti, 1989; Violanti D. et al., 1987). The lateral extent of the claystone-marl unit, its limited thickness (~40–80 m), and conformable contact with older shallow marine calcarenites indicate that deep marine conditions initiated around the same time over a large region. The claystone-marl unit thus records a short-lived period of accelerated subsidence and deepening that affected a large area of forearc crust between ~ 1.0 and 0.5 Ma.

The widespread extent of the change to rapid deepening requires a regional mechanism to draw down the crust that likely was related to dynamics of the Ionian subduction zone. Global sea-level rise is not a viable cause since the magnitude of documented deepening (500–1000 m) is much greater than the magnitude of Cenozoic sea-level fluctuations (100–150 m; Rohling et al., 2014; Siddall et al., 2003; Spratt and Lisiecki, 2016). Geodynamic processes that could have driven accelerated regional subsidence at ~ 1 Ma include crustal extension and thinning due to southeast retreat of the trench, increased density and related loading of the subducted Ionian slab, or intensification of convection in the mantle wedge above the descending slab. The subsequent change from regional subsidence to rapid post-0.5 Ma uplift may have been driven by laterally propagating slab tears and related toroidal flow in the upper mantle (Clementucci et al., 2024; Faccenna et al., 2011, 2014; Gallen et al., 2023).

5.3 Assessment of Paleoshoreline Modeling

Paleoshoreline modeling of uplifted marine terraces at Campo Piale ridge suggests an age of ~500–600 ka for the Piani di Melia terrace at 600–630 m elevation (Figs. 10, 11). Our analysis of fault-zone morphology shows that the Piani di Melia terrace correlates to the high SCA terrace at 1,000–1,200 m asl in the Piani di Aspromonte, and therefore the two terraces are the same age (Figs. 12-14). The terrace age inferred from shoreline modeling is slightly older than the maximum age permitted by $^{40}Ar/^{39}Ar$ dating of the Spadafora tuff (0.48 Ma) and thus represents an overestimate that may be due to several factors. First, the small difference between the isotopic age constraint (481 ± 19 ka) and shoreline model-based age (500–600 ka) could reflect the margin of error associated with highstand ages, since the age of each sea-level highstand has an uncertainty of ~± 5–10 ka (Rohling et al., 2014). When compounded over 8 sea-level highstands (Table 2), these uncertainties could potentially explain the difference between the $^{40}Ar/^{39}Ar$ age of the Spadafora tuff and the age estimate based on paleoshoreline modeling. Second, the paleoshoreline model does not account for any fault offsets, structural tilting, or fault-related warping along the modeled profile despite ample evidence for these processes in the study area (Figs. 1, 2, 12–14) and instead assumes uplift of a structurally intact undeformed crustal block. For each steep slope interpreted as a paleo-sea cliff that is instead a fault scarp, two adjacent terrace remnants would become the same age (Fig. 3), and the model age of the Piani di Melia surface would be reduced by the time span between highstands in the global sea-level record (Table 2; Rohling et al., 2014; Spratt & Lisiecki, 2016). Finally, Pavano et al.

(2024) obtained luminescence ages of ~330–210 ka in MGS deposits that underlie marine terrace sediments in NE Sicily, consistent with relative ages documented in the study area (Fig. 15a). However, this is not a compelling constraint because the luminescence ages are from a site located 25 – 30 km from dated sections southeast of Reggio Calabria (Fig. 4b), and the MGS in southern Calabria could be older than MGS in Sicily (Carbone, et al., 2022).

5.4 Summary

Our results challenge a long-standing assumption that higher-elevation terraces in southern Calabria are older, lower-elevation terraces are younger, and steep slopes between them are paleo-sea cliffs, not faults (Fig. 3). It can be difficult to interpret terraced landscapes using DEM analysis alone, because topographic scarps and risers are often rapidly degraded by the effects of uplift, erosion and local deposition in weakly consolidated sediments (e.g., Petit et al., 2009; Stewart and Hancock, 1988; Wallace, 1977). Future field-based studies that integrate geology, stratigraphy, geochronology, and tectonic geomorphology are needed to evaluate the relative role of paleo-sea cliffs versus fault scarps in shaping the structurally complex landscape of southern Calabria. This work is important for understanding Pleistocene paleogeography, drivers of crustal uplift and erosion, landscape response to faulting, and related geologic hazards in this seismically active region.

6 CONCLUSIONS

This study provides a new constraint on the age and uplift rates for faulted Pleistocene marine terraces in southern Calabria at elevations up to 1.0–1.3 km asl, as summarized below.

(1) $^{40}Ar/^{39}Ar$ dating of plagioclase and glass separates from a tuff in marine claystone of the Argille di Spadafora yield indistinguishable mean ages, with a more precise and more reliable age from step-heating experiments on glass of 0.481 ± 0.019 Ma (± 2σ).

(2) The Argille di Spadafora and equivalent Argille di Vito Superiore in southern Calabria, previously dated at ~ 1.0 – 0.5 Ma, are overlain by Messina Gravels and Sands Formation and capping Pleistocene marine terraces, and thus the marine terrace deposits are younger than 0.50 Ma.

(3) Paleoshoreline modeling at Campo Piale, Calabria, suggests an age of 525–590 ka for a terrace at 630 m asl. This is an overestimate because it assumes no fault offsets, tilting, or structural warping despite abundant geomorphic evidence for these processes in the study area.

(4) The 630-m terrace is correlated to the high SCA marine terrace at 1.0–1.3 km asl by tracing it up an active relay ramp between the Cittanova and Sant'Eufemia faults, and with geomorphic evidence for offset of the terrace across the Sant'Eufemia fault.

(5) The high-elevation SCA marine terrace is therefore < 0.50 Ma, roughly half a widely cited estimate of 1.0 ± 0.2 Ma. Our results suggest a time-averaged uplift rate of > 2.5 mm/y for the highest terrace and throw rates up to 1.0 mm/y on active normal faults.

(6) These findings challenge a common assumption that high-elevation terraces are older than lower-elevation terraces in southern Calabria, and suggest that the surface response to upper mantle processes may be faster than predicted in prior studies.

ACKNOWLEDGMENTS

Financial support for this research was provided to Dorsey by the University of Oregon, and logistical support was provided by the Università degli Studi della Basilicata. Andrea Dini is gratefully acknowledged for the acquisition of FE-SEM images. The Ar laserprobe facility was realized with the financial support of CNR. Meschis was supported by an INGV-led project (Idro1.RM task 1 9999.710 CR 7101 - Rete multiparametrica). Chiarella thanks Sval Energy for supporting the Fault-controlled deposits Phase 2 research project. *Tectonics* editor Taylor Schildgen and two anonymous reviewers are thanked for their constructive feedback that helped us improve the final version of the paper. Argibio S.r.l. is thanked for access to a clay quarry in Argille di Spadafora. We thank Charlie Ogle for valuable field assistance and logistical support of this study.

OPEN RESEARCH

Data Availability Statement: All $^{40}Ar/^{39}Ar$ data reported in this paper are available online at: https://doi.org/10.5880/fidgeo.2025.039 (Di Vincenzo et al., 2025). All DEMs and derivative slope maps and topographic profiles were extracted from Tinitaly 10-m digital elevation model, available at https://tinitaly.pi.ingv.it/ (Tarquini et al., 2023).

Conflict of Interest: The authors declare no conflicts of interest related to this study.

REFERENCES

Aïfa, T., Barrier, P., Feinberg, H. and Pozzi, J. P. (1987). Paléomagnétisme des terrains sédimentaires plio-quaternaires du Détroit de Messine. In *Le Detroit de Messine (Italie): Evolution tectono-sedimentaire récente (Pliocène et Quaternaire) et environment actuel* (pp. 83–90). Institut géologique Albert de Lapparent (IGAL).

Aïfa, T., Feinberg, H., & Pozzi, J. P. (1988). Pliocene-Pleistocene evolution of the Tyrrhenian arc: paleomagnetic determination of uplift and rotational deformation. *Earth and Planetary Science Letters*, *87*(4), 438–452. https://doi.org/10.1016/0012-821X(88)90007-6.

Aloisi, M., Bruno, V., Cannavò, F., Ferranti, L., Mattia, M., Monaco, C., & Palano, M. (2013). Are the source models of the M 7.1 1908 Messina Straits earthquake reliable? Insights from a novel inversion and a sensitivity analysis of levelling data. *Geophysical Journal International*, *192*(3), 1025–1041. https://doi.org/10.1093/gji/ggs062.

Andrenacci, C., Bello, S., Barbano Maria Serafina and de Nardis, R., Pirrotta, C., Pietrolungo, F., & Lavecchia, G. (2023). Reappraisal and analysis of macroseismic data for seismotectonic purposes: The strong earthquakes of southern Calabria, Italy. *Geosciences (Basel)*, *13*(7), 212. https://doi.org/10.3390/geosciences13070212.

Antonioli, F., Calcagnile, L., Ferranti, L., Mastronuzzi, G., Monaco, C., Orrù, P., Quarta, G., Pepe, F., Scardino, G., Scicchitano, G., Stocchi, P., & Taviani, M. (2021). New evidence of mis 3 relative sea level changes from the messina strait, Calabria (Italy). *Water (Switzerland)*, *13*(19). https://doi.org/10.3390/w13192647.

Antonioli, F., Ferranti, L., Lambeck, K., Kershaw, S., Verrubbi, V., & Dai Pra, G. (2006). Late Pleistocene to Holocene record of changing uplift rates in southern Calabria and northeastern Sicily (southern Italy, Central Mediterranean Sea). *Tectonophysics*, *422*(1–4), 23–40. https://doi.org/10.1016/j.tecto.2006.05.003.

Argnani, A. (2021). Comment on "New simulations and understanding of the 1908 Messina tsunami for a dual seismic and deep submarine mass failure source" by L. Schambach, S.T. Grilli, D.R. Tappin, M.D. Gangemi, G. Barbaro [Marine Geology 421 (2020) 106093]. In *Marine Geology* (Vol. 442). Elsevier B.V. https://doi.org/10.1016/j.margeo.2021.106634.

Argnani, A. (2022). Comment on the paper by Barreca et al.: "The Strait of Messina: Seismotectonics and the source of the 1908 earthquake" [Earth-Science Reviews 218, 2021, 103685]. In *Earth-Science Reviews* (Vol. 226). Elsevier B.V. https://doi.org/10.1016/j.earscirev.2022.103961.

Argnani, A., Brancolini, G., Bonazzi, C., Rovere, M., Accaino, F., Zgur, F., & Lodolo, E. (2009). The results of the Taormina 2006 seismic survey: Possible implications for active tectonics in the Messina Straits. *Tectonophysics*, *476*(1–2), 159–169. https://doi.org/10.1016/j.tecto.2008.10.029.

Armijo, R., Meyer, B., King, G. C. P., Rigo, A., & Papanastassiou, D. (1996). Quaternary evolution of the Corinth Rift and its implications for the Late Cenozoic evolution of the Aegean. *Geophysical Journal International*, *126*(1), 11–53. https://doi.org/10.1111/j.1365-246X.1996.tb05264.x.

Aykut, T., Yıldırım, C., Uysal, I. T., Ring, U., & Zhao, J. X. (2025). Coeval upper crustal extension and surface uplift in the Central Taurides (Türkiye) above the Cyprus Subduction Zone. *Nature Communications*, *16*(1). https://doi.org/10.1038/s41467-024-55802-w.

Balescu, S., Dumas, B., Guérémy, P., Lamothe, M., Lhénaff, R., & Raffy, J. (1997). Thermoluminescence dating tests of Pleistocene sediments from uplifted marine shorelines along the southwest coastline of the Calabrian Peninsula (southern Italy). *Palaeogeography, Palaeoclimatology, Palaeoecology*, *130*(1–4), 25–41. https://doi.org/10.1016/S0031-0182(96)00119-8.

Baratta, M. (1910). *La Catastrofe Sismica Calabro Messinese (28 Dicembre 1908).* Rome: Presso la Societa Geografica Italiana, 415 pp.

Barreca, G., Gross, F., Scarfì, L., Aloisi, M., Monaco, C., & Krastel, S. (2021). The Strait of Messina: Seismotectonics and the source of the 1908 earthquake. In *Earth-Science Reviews* (Vol. 218). Elsevier B.V. https://doi.org/10.1016/j.earscirev.2021.103685.

Barrier, P. (1984). *Evolution tectono-sédimentaire pliocène et pléistocène du Détroit de Messine (Italie)* [Ph.D. Dissertation]. Aix-Marseille University.

Barrier, P. (1986). Évolution paléogeographique du détroit de Messine au Pliocène et au Pléistocène. *Giornale Di Geologia*, *48*((1-2)), 7–24.

Barrier, P. (1987). Stratigraphie des depots pliocènes et quaternaires du Détroit de Messine. In *Le Detroit de Messine (Italy): Evolution tectono-sedimentaire récente (Pliocène et Quaternaire) et environment actuel: Vol. Doc. et Tr* (pp. 59–81). Institut Géologique Albert de Lapparent (IGAL).

Barrier, P., Alo, I. T., Geronimo, D. I., & Lanzafame, G. (1986). I rapporti tra tettonica e sedimentazione nell'evoluzione recente dell'Aspromonte Occidentale (Calabria). *Rivista Italiana Di Paleontologia e Stratigrafia*, *91*(4), 537–556.

Barrier, P., Casale, V., Costa, B., Di Geronimo, I., Oliveri, O., & Rosso, A. (1987). La sezione plio-pleistocenica di Pavigliana (Reggio Calabria). *Bollettino Della Società Paleontologica Italiana*, *25*(2), 107–144.

Barrier, P., & D'Alessandro, A. (1985). Structures biogèniques et physiques dans les Sabies de Pavigliana, Reggio Calabria (Italie). *Rivista Italiana Paleontologia e Stratigrafia*, *91*, 379–408.

Billi, A., Funiciello, R., Minelli, L., Faccenna, C., Neri, G., Orecchio, B., & Presti, D. (2008). On the cause of the 1908 Messina tsunami, southern Italy. *Geophys. Res. Lett.*, *35*(6). https://doi.org/10.1029/2008GL033251.

Billi, A., Minelli, L., Orecchio, B., & Presti, D. (2009). Runup distribution for the 1908 Messina tsunami in Italy: Observed data versus expected curves. *Bull. Seismol. Soc. Am.*, *99*(6), 3502–3509. https://doi.org/10.1785/0120090128.

Boschi, E., Pantosti, D., & Valensise, G. (1989). Modello di sorgente per il terremoto di Messina del 1908 ed evoluzione recente dell'area dello Stretto. *Atti VIII Convegno G. N.G.T.S.*, 245–258.

Brutto, F., Muto, F., Loreto, M. F., Paola, N. De, Tripodi, V., Critelli, S., & Facchin, L. (2016). The Neogene-Quaternary geodynamic evolution of the central Calabrian Arc: A case study from the western Catanzaro Trough basin. *Journal of Geodynamics*, *102*, 95–114. https://doi.org/10.1016/j.jog.2016.09.002.

Bucci, F., Santangelo, M., Fongo, L., Alvioli, M., Cardinali, M., & Melelli Laura and Marchesini, I. (2022). A new digital lithological map of Italy at the 1:100 000 scale for geomechanical modelling. *Earth Syst. Sci. Data*, *14*(9), 4129–4151. https://doi.org/10.5194/essd-14-4129-2022.

Carbone, S., Messina, A., & Lentini, F. (2022). *Note Illustrative della Carta geologica d'Italia alla scala 1:50.000 F. 601 Messina - Reggio di Calabria. Servizio Geologico d'Italia*. INFN Open Access Repository. https://doi.org/10.15161/oar.it/76891.

Catalano, S., & De Guidi, G. (2003). Late Quaternary uplift of northeastern Sicily: Relation with the active normal faulting deformation. *Journal of Geodynamics*, *36*(4), 445–467. https://doi.org/10.1016/S0264-3707(02)00035-2.

Catalano, S., De Guidi, G., Monaco, C., Tortorici, G., & Tortorici, L. (2008). Active faulting and seismicity along the Siculo-Calabrian Rift Zone (Southern Italy). *Tectonophysics*, *453*(1–4), 177–192. https://doi.org/10.1016/j.tecto.2007.05.008.

Cavazza, W., & Longhitano, S. G. (2023). Palaeostrait tectonosedimentary facies during late Cenozoic microplate rifting and dispersal in the western Mediterranean. *Geological Society Special Publication*, *523*(1), 399–426. https://doi.org/10.1144/SP523-2021-95.

Cerrone, C., Meschis, M., Ascione, A., Soligo, M., Tuccimei, P., Robertson, J., & Roberts, G. P. (2025). Tectonic implications of raised Quaternary relative sea-level indicators along the NE border of the Campania Plain (southern Italy). *Earth Surf. Process.*, *50*(1). https://doi.org/10.1002/esp.6066.

Cerrone, C., Vacchi, M., Fontana, A., & Rovere, A. (2021). Last Interglacial sea-level proxies in the western Mediterranean. *Earth Syst. Sci. Data*, *13*(9), 4485–4527. https://doi.org/10.5194/essd-13-4485-2021.

Chiarella, D., Capella, W., Longhitano, S. G., & Muto, F. (2021). Fault-controlled base-of-scarp deposits. *Basin Research*, *33*(2), 1056–1075. https://doi.org/10.1111/bre.12505.

Childs, C., Worthington, R. P., Walsh, J. J., & Roche, V. (2019). Conjugate relay zones: geometry of displacement transfer between opposed-dipping normal faults. *Journal of Structural Geology*, *118*, 377–390. https://doi.org/10.1016/j.jsg.2018.11.007.

Cirrincione, R., Fazio, E., Fiannacca, P., Ortolano, G., Pezzino, A., & Punturo, R. (2015). The Calabria-Peloritani Orogen, a composite terrane in Central Mediterranean; Its overall architecture and geodynamic significance for a pre-Alpine scenario around the Tethyan basin. *Periodico Di Mineralogia*, *84*(3B). https://doi.org/10.2451/2015PM0446.

Clementucci, R., Lanari, R., Faccenna, C., Crosetto, S., Reitano, R., Zoppis, G., & Ballato, P. (2024). Morpho-tectonic evolution of the Southern Apennines and Calabrian arc: Insights from Pollino range and surrounding extensional intermontane basins. *Tectonics*, *43*(5). https://doi.org/10.1029/2023TC008002.

Comerci, V., Vittori, E., Blumetti, A. M., Brustia, E., Di Manna, P., Guerrieri, L., Lucarini, M., & Serva, L. (2015). Environmental effects of the December 28, 1908, Southern Calabria–Messina (Southern Italy) earthquake. *Nat. Hazards (Dordr.)*, *76*(3), 1849–1891. https://doi.org/10.1007/s11069-014-1573-x.

Cornette, Y., Gillot, P.-Y., Barrier, P., & Jehenne, F. (1987). Donnees radiometriques preliminaires (Potassium-Argon) sur des cinerites plio-pleistocenes du Detroit de Messine. In *Le Detroit de Messine (Italy): Evolution tectono-sedimentaire récente (Pliocène et Quaternaire) et environment actuel: Vol. Doc. et Travaux, 11* (pp. 97–100). , Institut Geologique Albert De Lapparent (IGAL).

Costantini, E. A. C., & Dazzi, C. (2013). *The Soils of Italy* (World Soil, Issue January 2013). Springer Science + Business. https://doi.org/10.1007/978-94-007-5642-7.

Cowie, P. A., Gupta, S., & Dawers, N. H. (2000). Implications of fault array evolution for synrift depocentre development: insights from a numerical fault growth model. *Basin Res.*, *12*(3–4), 241–261. https://doi.org/10.1111/j.1365-2117.2000.00126.x.

Cowie, P. A., & Roberts, G. P. (2001). Constraining slip rates and spacings for active normal faults. *Journal of Structural Geology*, *23*(12), 1901–1915. https://doi.org/10.1016/S0191-8141(01)00036-0.

Crippa, G., Angiolini, L., Bottini, C., Erba, E., Felletti, F., Frigerio, C., Hennissen, J. A. I., Leng, M. J., Petrizzo, M. R., Raffi, I., Raineri, G., & Stephenson, M. H. (2016). Seasonality fluctuations recorded in fossil bivalves during the early Pleistocene: Implications for climate change. *Palaeogeography, Palaeoclimatology, Palaeoecology*, *446*, 234–251. https://doi.org/10.1016/j.palaeo.2016.01.029.

de Gelder, G., Fernández-Blanco, D., Melnick, D., Duclaux, G., Bell, R. E., Jara-Muñoz, J., Armijo, R., & Lacassin, R. (2019). Lithospheric flexure and rheology determined by climate cycle markers in the Corinth Rift. *Scientific Reports*, *9*(1), 1–12. https://doi.org/10.1038/s41598-018-36377-1.

de Gelder, G., Fernández-Blanco, D., Öğretmen, N., Liakopoulos, S., Papanastassiou, D., Faranda, C., Armijo, R., & Lacassin, R. (2022). Quaternary E-W Extension Uplifts Kythira Island and Segments the Hellenic Arc. *Tectonics*, *41*(10), 1–24. https://doi.org/10.1029/2022TC007231.

De Guidi, G., Catalano, S., Monaco, C., & Tortorici, L. (2003). Morphological evidence of Holocene coseismic deformation in the Taormina region (NE Sicily). *Journal of Geodynamics*, *36*(1–2), 193–211. https://doi.org/10.1016/S0264-3707(03)00047-4.

De Rosa, R., Dominici, R., Donato, P., & Barca, D. (2008). Widespread syn-eruptive volcaniclastic deposits in the Pleistocenic basins of South-Western Calabria. *J. Volcanol. Geotherm. Res.*, *177*(1), 155–169. https://doi.org/10.1016/j.jvolgeores.2007.11.011.

De Santis, V., Cerrone, C., Meschis, M., Scicchitano, G., Ascione, A., & Caldara, M. (2025). Reoccupation of late Quaternary relative sea level indicators in a tectonically quasi-stable coastal area in Southern Italy (Cilento headland): Insights into the Last Interglacial stillstands. *Geomorphology (Amst.)*, *478*(109692), 109692. https://doi.org/10.1016/j.geomorph.2025.109692.

De Santis, V., Scardino, G., Meschis Marco and Ortiz, J. E., Sánchez-Palencia, Y., & Caldara, M. (2021). Refining the middle-late Pleistocene chronology of marine terraces and uplift history in a sector of the Apulian foreland (southern Italy) by applying a synchronous correlation technique and amino acid racemization to Patella spp. and Thetystrombus latus. *Ital. J. Geosci.*, *140*(3), 438–463. https://doi.org/10.3301/IJG.2021.05.

De Santis, V., Scardino, G., Scicchitano, G., Meschis, M., Montagna, P., Pons-Branchu, E., Ortiz, J. E., Sánchez-Palencia, Y., & Caldara, M. (2023). Middle-late Pleistocene chronology of palaeoshorelines and uplift history in the low-rising to stable Apulian foreland: Overprinting and reoccupation. *Geomorphology (Amst.)*, *421*(108530), 108530. https://doi.org/10.1016/j.geomorph.2022.108530.

Di Bella, M., Italiano, F., Sabatino, G., Tripodo, A., Baldanza, A., Casella, S., Pino, P., Rasa', R., & Russo, S. (2016). Pleistocene volcaniclastic units from North-Eastern Sicily (Italy): new evidence for calc-alkaline explosive volcanism in the Southern Tyrrhenian Sea. *Geol. Carpath.*, *67*(4), 371–389. https://doi.org/10.1515/geoca-2016-0023.

Di Geronimo, I., D'Atri, A., La Perna, R., Rosso, A., Sanfilippo, R., & Violanti, D. (1997). The Pleistocene bathyal section of Archi (Southern Italy). *Bollettino Soc. Paleontologica Italiana*, *36*, 189–212.

Di Stefano, A., Baldassini, N., Raffi Isabella and Fornaciari, E., Incarbona, A., Negri, A., Bonomo, S., Villa, G., Di Stefano, E., & Rio, D. (2023). Neogene-Quaternary Mediterranean calcareous nannofossil biozonation and biochronology: A review. *Stratigraphy*, *20*(4), 259–302. https://doi.org/10.29041/strat.20.4.02.

Di Stefano, A., & Lentini, R. (1995). Ricostruzione stratigrafica e significato paleotettonico dei depositi plio-pleistocenici del margine tirrenico tra Villafranca Tirrena e Faro (Sicilia nord-orientale). *Studi Geologici Camerti*, *2*, 219–237.

Di Stefano, A., & Longhitano, S. (2009). Tectonics and sedimentation of the Lower and Middle Pleistocene mixed siliciclastic/bioclastic sedimentary successions of the Ionian Peloritani Mts (NE Sicily, Southern Italy): The onset of opening of the Messina Strait. *Central European Journal of Geosciences*, *1*(1), 33–62. https://doi.org/10.2478/v10085-009-0002-y.

Di Stefano, A., Longhitano, S., & Smedile, A. (2007). Sedimentation and tectonics in a steep shallow-marine depositional system: stratigraphic arrangement of the Pliocene-Pleistocene Rometta Succession (NE Sicily, Italy). *Geologica Carpathica*, *58*(1), 71–87. https://www.researchgate.net/publication/278782708.

Di Vincenzo, G. (2022). High precision multi-collector 40Ar/39Ar dating of moldavites (Central European tektites) reconciles geochrological and paleomagnetic data. *Chem. Geol.*, *608*(121026), 121026. https://doi.org/10.1016/j.chemgeo.2022.121026.

Di Vincenzo, G., Dorsey, R. J., Meschis, M., Longhitano, S. G., Cavazza, W., & Chiarella, D. (2025). *Multi-collector 40Ar/39Ar data of glass and plagioclase from a tuff sample in the marine claystone of the Argille di Spadafora (NE Sicily, Italy) [Dataset]*. https://doi.org/10.5880/fidgeo.2025.039.

Di Vincenzo, G., Folco, L., Suttle, M. D., Brase, L., & Harvey, R. P. (2021). Multi-collector 40Ar/39Ar dating of microtektites from Transantarctic Mountains (Antarctica): A definitive link with the Australasian tektite/microtektite strewn field. *Geochimica et Cosmochimica Acta*, *298*, 112–130. https://doi.org/10.1016/j.gca.2021.01.046.

Dorsey, R. J., Longhitano, S. G., & Chiarella, D. (2024). Structure and morphology of an active conjugate relay zone, Messina Strait, southern Italy. *Basin Res.*, *36*(1). https://doi.org/10.1111/bre.12818.

Dumas, B., Gueremy, P., Hearty, P. J., Lhenaff, R., & Raffy, J. (1988). Morphometric analysis and amino acid geochronology of uplifted shorelines in a tectonic region near reggio Calambria, South Italy.

Palaeogeogr. Palaeoclimatol. Palaeoecol., *68*(2–4), 273–289. https://doi.org/10.1016/0031-0182(88)90045-4.

Dumas, B., Gueremy, P., Lhenaff, R., & Raffy, J. (1987). Rates of uplift as shown by raised Quaternary shorelines in Southern Calabria (Italy). *Zeitschrift Für Geomorphologie. Supplementband*, *63*, 119–132.

Dumas, B., Guérémy, P., Lhénaff, R., & Raffy, J. (2000). Périodicités de temps long et de temps court, depuis 400 000 ans, dans l'étagement des terrasses marines en Calabre méridionale (Italie) / Long and short timing from 400000 years in the stepped marine terraces in Southern Calabria (Italy). *Géomorphologie Relief Processus Environnement*, *6*(1), 25–44. https://doi.org/10.3406/morfo.2000.1041.

Dumas, B., Gueremy, P., Lhenaff, R., & Raffy, J. ,. (1981). Le soulèvement quaternaire de la Calabrie méridionale. *Revue de Géologie Dynamique et de Géographie Physique Paris*, *23*(1), 27–40.

Dumas, B., Guérémy, P., & Raffy, J. (2005). Evidence for sea-level oscillations by the ``characteristic thickness'' of marine deposits from raised terraces of Southern Calabria (Italy). *Quat. Sci. Rev.*, *24*(18–19), 2120–2136. https://doi.org/10.1016/j.quascirev.2004.12.011.

Dumas, B., & Raffy, J. (2006). How eustatic raised marine terraces of Calabria can be connected with climate oscillations occurring over the MIS 5-MIS 4 period. *Geografia Fisica e Dinamica Quaternaria*, *29*(1), 11–31.

Faccenna, C., Becker, T. W., Miller Meghan S and Serpelloni, E., & Willett, S. D. (2014). Isostasy, dynamic topography, and the elevation of the Apennines of Italy. *Earth Planet. Sci. Lett.*, *407*, 163–174. https://doi.org/10.1016/j.epsl.2014.09.027.

Faccenna, C., Molin, P., Orecchio, B., Olivetti, V., Bellier, O., Funiciello, F., Minelli, L., Piromallo, C., & Billi, A. (2011). Topography of the Calabria subduction zone (southern Italy): Clues for the origin of Mt. Etna. *Tectonics*, *30*(1). https://doi.org/10.1029/2010TC002694.

Favalli, M., Boschi, E., & Mazzarini Francesco and Pareschi, M. T. (2009). Seismic and landslide source of the 1908 Straits of Messina tsunami (Sicily, Italy). *Geophys. Res. Lett.*, *36*(16). https://doi.org/10.1029/2009GL039135.

Fernández-Blanco, D., de Gelder, G., Lacassin, R., & Armijo, R. (2019). A new crustal fault formed the modern Corinth Rift. *Earth-Science Reviews*, *199*(February), 102919. https://doi.org/10.1016/j.earscirev.2019.102919.

Ferranti, L., Antonioli, F., Mauz, B., Amorosi, A., Dai Pra, G., Mastronuzzi, G., Monaco, C., Orrù, P., Pappalardo, M., Radtke, U., Renda, P., Romano, P., Sansò, P., & Verrubbi, V. (2006). Markers of the last interglacial sea-level high stand along the coast of Italy: Tectonic implications. *Quaternary International*, *145–146*, 30–54. https://doi.org/10.1016/j.quaint.2005.07.009.

Ferranti, L., Antonioli, F., Monaco, C., Scicchitano, G., & Spampinato, C. R. (2017). Uplifted Late Holocene shorelines along the coasts of the Calabrian Arc: Geodynamic and seismotectonic implications. *Italian Journal of Geosciences*, *136*(3), 454–470. https://doi.org/10.3301/IJG.2017.13.

Ferranti, L., Monaco, C., Antonioli, F., Maschio, L., Kershaw, S., & Verrubbi, V. (2007). The contribution of regional uplift and coseismic slip to the vertical crustal motion in the Messina Straits, southern Italy: Evidence from raised Late Holocene shorelines. *Journal of Geophysical Research: Solid Earth*, *112*(6). https://doi.org/10.1029/2006JB004473.

Finch, E., & Gawthorpe, R. (2017). Growth and interaction of normal faults and fault network evolution in rifts: Insights from three-dimensional discrete element modelling. In *Geological Society Special Publication* (Vol. 439, Issue 1, pp. 219–248). Geological Society of London. https://doi.org/10.1144/SP439.23.

Ford, M., Hemelsdaël, R., Mancini, M., & Palyvos, N. (2017). Rift migration and lateral propagation: Evolution of normal faults and sediment-routing systems of the western Corinth rift (Greece). In *Geological Society Special Publication* (Vol. 439, Issue 1). https://doi.org/10.1144/SP439.15.

Fossen, H., & Rotevatn, A. (2016). Fault linkage and relay structures in extensional settings-A review. In *Earth-Science Reviews* (Vol. 154, pp. 14–28). Elsevier. https://doi.org/10.1016/j.earscirev.2015.11.014.

Gallen, S. F., Seymour, N. M., Glotzbach, C., Stockli, D. F., & O'Sullivan, P. (2023). Calabrian forearc uplift paced by slab–mantle interactions during subduction retreat. *Nature Geoscience*, *16*(6), 513–520. https://doi.org/10.1038/s41561-023-01185-4.

Galli, P., & Bosi, V. (2002). Paleoseismology along the Cittanova fault: Implications for seismotectonics and earthquake recurrence in Calabria (southern Italy). *J. Geophys. Res.*, *107*(B3). https://doi.org/10.1029/2001JB000234.

Galli, P., Galadini, F., & Pantosti, D. (2008). Twenty years of paleoseismology in Italy. *Earth Sci. Rev.*, *88*(1–2), 89–117. https://doi.org/10.1016/j.earscirev.2008.01.001.

Geograficzne, P. (2011). *Kalliopi Gaki-Papanastassiou , Hampik Maroukian , and Violeta Kourmpanian THE MORPHOTECTONIC EVOLUTION OF THE SOUTHERN HALF OF KYTHIRA ISLAND (IONIAN SEA , GREECE) Kythira is located in southern Greece between southern Peloponnese and Cre-*. 49–60.

Ghisetti, F. (1981). Upper Pliocene-Pleistocene uplift rates as indicators of neotectonic pattern: an example from southern Calabria (Italy). *Zeitschrift Fur Geomorphologie*, *40*, 93–118.

Ghisetti, F., Vezzani, L., Pezzino, A., & Atzori, P. (1983). *Carta geologica del bordo occidentale dell'Aspromonte, Scale 1:50,000*. https://www.pconti.net/egeo_results.php?id=null171.

Girone, A. (2003). The Pleistocene bathyal teleostean fauna of Archi (southern Italy): Palaeoecological and palaeobiogeographic implications. *Rivista Italiana Di Paleontologia e Stratigrafia*, *109*(1), 99–110. https://doi.org/10.13130/2039-4942/5496.

Goldsworthy, M., & Jackson, J. (2000). Active normal fault evolution in Greece revealed by geomorphology and drainage patterns. In *Journal of the Geological Society* (Vol. 157).

Goldsworthy, M., & Jackson, J. (2001). Migration of activity within normal fault systems: examples from the Quaternary of mainland Greece. *Journal of Structural Geology*, *23*(2–3), 489–506. www.elsevier.nl/locate/jstrugeo.

Guarnieri, P., Di Stefano, A., Carbone, S., Lentini, F., & Del Ben, A. (2004). A multidisciplinary approach to the reconstruction of the Quaternary evolution of the Messina Strait (including: Geological Map of the Messina Strait area, scale 1: 25.000). In *Mapping Geology of Italy (2005)* (pp. 44–50).

Holtmann, R., Cattin, R., Simoes, M., & Steer, P. (2023). Revealing the hidden signature of fault slip history in the morphology of degrading scarps. *Sci. Rep.*, *13*(1), 3856. https://doi.org/10.1038/s41598-023-30772-z.

Houghton, S. L., Roberts, G. P., Papanikolaou, I. D., McArthur, J. M., & Gilmour, M. A. (2003). New ^234U-^230Th coral dates from the western Gulf of Corinth: Implications for extensional tectonics. *Geophys. Res. Lett.*, *30*(19). https://doi.org/10.1029/2003GL018112.

Jacques, E., Monaco, C., Tapponnier, P., Tortorici, L., & Winter, T. (2001). Faulting and earthquake triggering during the 1783 Calabria seismic sequence. *Geophysical Journal International*, *147*(3), 499–516. https://doi.org/10.1046/j.0956-540x.2001.01518.x.

Khalil, S. M., & McClay, K. R. (2017). 3D geometry and kinematic evolution of extensional fault-related folds, NW Red Sea, Egypt. *Geological Society, London, Special Publications*, *439*(1), 109–130. https://doi.org/10.1144/SP439.11.

Lavecchia, G., Bello, S., Andrenacci, C., Cirillo, D., Pietrolungo, F., Talone Donato and Ferrarini, F., de Nardis, R., Galli, P., Faure Walker, J., Sgambato, C., Menichetti Marco and Monaco, C., Gambino, S., De Guidi Giorgio and Barreca, G., Carnemolla, F., Brighenti, F., Giuffrida, S., Pirrotta, C., Carboni, F., Ferranti, L., … Roberts Gerald and Brozzetti, F. (2024). QUIN 2.0 - new release of the QUaternary fault strain INdicators database from the Southern Apennines of Italy. *Sci. Data*, *11*(1), 189. https://doi.org/10.1038/s41597-024-03008-6.

Lee, J.-Y., Marti, K., Severinghaus, J. P., Kawamura, K., Yoo, H.-S., Lee, J. B., & Kim, J. S. (2006). A redetermination of the isotopic abundances of atmospheric Ar. *Geochim. Cosmochim. Acta*, *70*(17), 4507–4512. https://doi.org/https://doi.org/10.1016/j.gca.2006.06.1563.

Lentini, F., Carbone, S., Catalano, S., Di Stefano, A., Gargano, C., Romeo, M., Strazzulla, S., & Vinci, G. (1995). Sedimentary evolution of basins in mobile belts: examples from the Tertiary terrigenous sequences of the Peloritani Mountains (NE Sicily). *Terra Nova*, *7*(2), 161–170. https://doi.org/10.1111/j.1365-3121.1995.tb00685.x.

Lentini, F., Catalano, S., & Carbone, S. (2000). *Geological map of Messina province (NE Sicily), scale 1:50.000*.

Longhitano, S. G. (2018). Between Scylla and Charybdis (part 2): The sedimentary dynamics of the ancient, Early Pleistocene Messina Strait (central Mediterranean) based on its modern analogue. In *Earth-Science Reviews* (Vol. 179, pp. 248–286). Elsevier B.V. https://doi.org/10.1016/j.earscirev.2018.01.017.

Longhitano, S. G., Chiarella, D., Di Stefano, A., Messina, C., Sabato, L., & Tropeano, M. (2012). Tidal signatures in Neogene to Quaternary mixed deposits of southern Italy straits and bays. *Sedimentary Geology*, *279*, 74–96. https://doi.org/10.1016/j.sedgeo.2011.04.019.

Mearns, E., & Sornette, D. (2021). A transfer fault complex to explain the geodynamics and faulting mechanisms of the 1976 M7.8 Tangshan earthquake China. *J. Asian Earth Sci.*, *213*(104738), 104738. https://doi.org/10.1016/j.jseaes.2021.104738.

Mercier, D., Barrier, P., Beaudoin, B., Didier, S., Montenat, J. L., & Salinas Zuniga, E. (1987). Les facteurs hydrodynamiques dans la sedimentazion plio-quaternaire du Détroit de Messine. In *Le Detroit de Messine (Italy): Evolution tectono-sedimentaire récente (Pliocène et Quaternaire) et environment actuel: Vol. Doc. et Travaux, 11* (pp. 171–183). Institut Geologique Albert De Lapparent (IGAL).

Meschis, M., Roberts, G. P., Mildon, Z. K., Robertson, J., Michetti, A. M., & Faure Walker, J. P. (2019). Slip on a mapped normal fault for the 28 th December 1908 Messina earthquake (Mw 7.1) in Italy. *Scientific Reports*, *9*(1). https://doi.org/10.1038/s41598-019-42915-2.

Meschis, M., Roberts, G. P., Robertson, J., & Briant, R. M. (2018). The relationships between regional Quaternary uplift, deformation across active normal faults, and historical seismicity in the upper plate of subduction zones: The Capo D'Orlando Fault, NE Sicily. *Tectonics*, *37*(5), 1231–1255. https://doi.org/10.1029/2017TC004705.

Meschis, M., Roberts, G. P., Robertson, J., Mildon, Z. K., Sahy, D., Goswami, R., Sgambato, C., Walker, J. F., Michetti, A. M., & Iezzi, F. (2022). Out of phase Quaternary uplift-rate changes reveal normal fault interaction, implied by deformed marine palaeoshorelines. *Geomorphology*, *416*. https://doi.org/10.1016/j.geomorph.2022.108432.

Meschis, M., Romano, D., Palano, M., Scicchitano, G., De Santis, V., Scardino, G., Gattuso, A., Caruso, C. G., Sposito, F., Lazzaro, G., Scappuzzo, S. S. S., Semprebello, A., Morici, S., & Longo, M. (2024). Crustal uplift rates implied by synchronously investigating Late Quaternary marine terraces in the Milazzo Peninsula, Northeast Sicily, Italy. *Earth Surf. Process.*, *49*(11), 3555–3574. https://doi.org/10.1002/esp.5922.

Meschis, M., Scicchitano, G., Roberts, G. P., Robertson J and Barreca, G., Monaco, C., Spampinato, C., Sahy, D., Antonioli, F., Mildon, Z. K., & Scardino, G. (2020). Regional deformation and offshore crustal local faulting as combined processes to explain uplift through time constrained by investigating differentially uplifted Late Quaternary paleoshorelines: The foreland Hyblean Plateau, SE Sicily. *Tectonics*, *39*(12). https://doi.org/10.1029/2020TC006187.

Messina, C., Rosso, M. A., Sciuto Francesco and Di Geronimo, I., Nemec, W., Di Dio Tatiana and Di Geronimo, R., Maniscalco, R., & Sanfilippo, R. (2009). Anatomy of a transgressive systems tract revealed by integrated sedimentological and palaeoecological study: The barcellona Pozzo Di gotto

basin, northeastern Sicily, Italy. In *Sedimentary Processes, Environments and Basins* (pp. 367–400). Blackwell Publishing Ltd. https://doi.org/10.1002/9781444304411.ch17.

Min, K., Mundil, R., Renne, P. R., & Ludwig, K. R. (2000). A test for systematic errors in 40Ar/39Ar geochronology through comparison with U/Pb analysis of a 1.1-Ga rhyolite. *Geochimica et Cosmochimica Acta*, *64*(1), 73–98. https://doi.org/10.1016/S0016-7037(99)00204-5.

Miyauchi, T. (1994). Geochronology of Pleistocene marine terraces and regional tectonics in the Tyrrhenian coast of South Calabria. *Il Quaernario*, *7*, 17–34. https://doi.org/10.26382/.

Monaco, C., Barreca, G., & Di Stefano, A. (2017). Quaternary marine terraces and fault activity in the northern mainland sectors of the Messina Strait (southern Italy). *Italian Journal of Geosciences*, *136*(3), 337–346. https://doi.org/10.3301/IJG.2016.10.

Monaco, C., Tapponnier, P., Tortorici, L., & Gillot ', P. Y. (1997). Late Quaternary slip rates on the Acireale-Piedimonte normal faults and tectonic origin of Mt. Etna (Sicily). In *EPSL Earth and Planetary Science Letters* (Vol. 147). https://doi.org/10.1016/S0012-821X(97)00005-8.

Monaco, C., & Tortorici, L. (2000). Active faulting in the Calabrian arc and eastern Sicily. *Journal of Geodynamics*, *29*(3–5), 407–424. https://doi.org/10.1016/S0264-3707(99)00052-6.

Monaco, C., Tortorici, L., Nicolich, R., Cemobori, L., & Costa, M. (1996). From collisional to rifted basins: an example from the southern Calabrian arc (Italy). In *Tectonophysics* (Vol. 266). https://doi.org/10.1016/S0040-1951(96)00192-8.

Neri, G., Orecchio, B., Scolaro, S., & Totaro, C. (2020). Major Earthquakes of Southern Calabria, Italy, Into the Regional Geodynamic Context. *Frontiers in Earth Science*, *8*. https://doi.org/10.3389/feart.2020.579846.

Niespolo, E. M., Rutte, D., Deino, A. L., & Renne, P. R. (2017). Intercalibration and age of the Alder Creek sanidine 40Ar/39Ar standard. *Quat. Geochronol.*, *39*, 205–213. https://doi.org/10.1016/j.quageo.2016.09.004.

Ogg, J. G. (2020). Geomagnetic polarity time scale. In *Geologic Time Scale 2020* (pp. 159–192). Elsevier. https://doi.org/10.1016/B978-0-12-824360-2.00005-X.

Ogniben, L. (1960). Explicative notes of the geological scheme of NE Sicily. *Rivista Mineraria Siciliana*, *64*, 183–212.

Öğretmen, N., Cipollari, P., Frezza, V., Faranda, C., Karanika, K., Gliozzi, E., Radeff, G., & Cosentino, D. (2018). Evidence for 1.5 km of Uplift of the Central Anatolian Plateau's Southern Margin in the Last 450 kyr and Implications for Its Multiphased Uplift History. *Tectonics*, *37*(1), 359–390. https://doi.org/10.1002/2017TC004805.

Palano, M., Ferranti, L., Monaco, C., Mattia, M., Aloisi, M., Bruno, V., Cannav, F., & Siligato, G. (2012). GPS velocity and strain fields in Sicily and southern Calabria, Italy: Updated geodetic constraints on tectonic block interaction in the central Mediterranean. *Journal of Geophysical Research: Solid Earth*, *117*(7). https://doi.org/10.1029/2012JB009254.

Palano, M., Piromallo, C., & Chiarabba, C. (2017). Surface imprint of toroidal flow at retreating slab edges: The first geodetic evidence in the Calabrian subduction system. *Geophysical Research Letters*, *44*(2), 845–853. https://doi.org/10.1002/2016GL071452.

Pan, S., Bell, R. E., Jackson, C. A.-L., & Naliboff, J. (2022). Evolution of normal fault displacement and length as continental lithosphere stretches. *Basin Res.*, *34*(1), 121–140. https://doi.org/10.1111/bre.12613.

Pavano, F. (2025). Fault geometry, strain partitioning and deformation history inferred by fluvial topography and marine terraces analyses. *Geomorphology (Amst.)*, *472*(109583), 109583. https://doi.org/10.1016/j.geomorph.2024.109583.

Pavano, F., Pazzaglia, F. J., & Catalano, S. (2016). Knickpoints as geomorphic markers of active tectonics: A case study from northeastern Sicily (southern Italy). *Lithosphere*, *8*(6), 633–648. https://doi.org/10.1130/L577.1.

Pavano, F., Pazzaglia, F. J., Rittenour, T. M., Catalano S and Corbett, L. B., & Bierman, P. (2024). Integrated uplift, subsidence, erosion and deposition in a tightly coupled source-to-sink system, Pagliara basin, northeastern Sicily, Italy. *Basin Res.*, *36*(1). https://doi.org/10.1111/bre.12845.

Peacock, D. C. P., & Sanderson, D. J. (1991). Displacements, segment linkage and relay ramps in normal fault zones. *Journal of Structural Geology*, *13*(6), 721–733. https://doi.org/10.1016/0191-8141(91)90033-F.

Peacock, D. C., & Sanderson, D. J. (1994). Geometry and development of relay ramps in normal fault systems. *AAPG Bulletin*, *78*(2), 147–165. https://doi.org/10.1306/BDFF9046-1718-11D7-8645000102C1865D.

Pedoja, K., Jara-Muñoz, J., De Gelder, G., Robertson, J., Meschis, M., Fernandez-Blanco, D., Nexer, M., Poprawski, Y., Dugué, O., Delcaillau, B., Bessin P and Benabdelouahed, M., Authemayou, C., Husson, L., Regard, V., Menier, D., & Pinel, B. (2018). Neogene-Quaternary slow coastal uplift of Western Europe through the perspective of sequences of strandlines from the Cotentin Peninsula (Normandy, France). *Geomorphology (Amst.)*, *303*, 338–356. https://doi.org/10.1016/j.geomorph.2017.11.021.

Perez, A., Gallen, S. F., Heizler, M. T., Ricci, J., Ghamedi, O. M., Giachetta, E., & Molin, P. (2024, December 10). New 40 Ar/39 Ar Detrital Sanidine Geochronology of Marine Terraces in Southern Italy: Implications for Quaternary Uplift Rates and Geodynamics in the Calabrian Arc. *AGU24*.

Petit, C., Gunnell, Y., Gonga-Saholiariliva, N., Meyer, B., & Séguinot, J. (2009). Faceted spurs at normal fault scarps: Insights from numerical modeling. *Journal of Geophysical Research: Solid Earth*, *114*(5). https://doi.org/10.1029/2008JB005955.

Pino, P., Baldanza, A., Belfiore, C., Di Bella, M., Sabatino, G., & Triscari, M. (2007). Pleistocene clay formations in the Messina country (N.E. Sicily): a stratigraphic review. *Plinius, FIST 2007, Rimini, Epitome*, 401–401.

Pino, P., Belfiore, C., Casella, S., Di Bella, M., Rasa, R., Sabatino, G., Tripodo, A., & Triscari, M. (2007). Interbedded ash levels in Pleistocene clay formations of the Tyrrhenian coast of Sicily: possible archaeometric implications. *6th Italian Earth Sciences Forum, Geoitalia 2007, Epitome*, 343–344.

Pirrotta, C., Barberi, G., Barreca, G., Brighenti, F., Carnemolla, F., De Guidi, G., Monaco, C., Pepe, F., & Scarfì, L. (2021). Recent activity and kinematics of the bounding faults of the catanzaro trough (Central calabria, italy): New morphotectonic, geodetic and seismological data. *Geosciences (Switzerland)*, *11*(10). https://doi.org/10.3390/geosciences11100405.

Pirrotta, C., Parrino, N., Pepe, F., Tansi, C., & Monaco, C. (2022). Geomorphological and Morphometric Analyses of the Catanzaro Trough (Central Calabrian Arc, Southern Italy): Seismotectonic Implications. *Geosciences (Switzerland)*, *12*(9). https://doi.org/10.3390/geosciences12090324.

Presti, D., Totaro, C., Neri, G., & Orecchio, B. (2019). New earthquake data in the Calabrian subduction zone, Italy, suggest revision of the presumed dynamics in the upper part of the subducting slab. *Seismological Research Letters*, *90*(5), 1994–2004. https://doi.org/10.1785/0220190024.

Quye-Sawyer, J., Whittaker, A. C., Roberts, G. G., & Rood, D. H. (2021). Fault Throw and Regional Uplift Histories From Drainage Analysis: Evolution of Southern Italy. *Tectonics*, *40*(4). https://doi.org/10.1029/2020TC006076.

Racano, S., Schildgen, T. F., Cosentino, D., & Miller, S. R. (2021). Temporal and Spatial Variations in Rock Uplift From River-Profile Inversions at the Central Anatolian Plateau Southern Margin. *Journal of Geophysical Research: Earth Surface*, *126*(8). https://doi.org/10.1029/2020JF006027.

Rio, D., Raffi, I., Villa, G., & Kastens, K. A. (1990). Pliocene-Pleistocene calcareous nannofossil distribution patterns in the western Mediterranean. *Proceedings of the Ocean Drilling Program, Scientific Results* , *107*, 513–533.

Rivieccio, R. (2020). *Soil Database of Italy at 1:250, 000 Scale and Thematic Applications for Assessing Environmental Services* [Università degli Studi della Tuscia di Viterbo]. http://hdl.handle.net/2067/49539.

Roberts, G. P., Houghton, S. L., Underwood, C., Papanikolaou, I., Cowie, P. A., Van Calsteren, P., Wigley, T., Cooper, F. J., & McArthur, J. M. (2009). Localization of quaternary slip rates in an active rift in 105 years: An example from central Greece constrained by 234U- 230Th coral dates from uplifted paleoshorelines. *Journal of Geophysical Research: Solid Earth*, *114*(10). https://doi.org/10.1029/2008JB005818.

Roberts, G. P., Meschis, M., Houghton, S., Underwood, C., & Briant, R. M. (2013). The implications of revised Quaternary palaeoshoreline chronologies for the rates of active extension and uplift in the upper plate of subduction zones. *Quaternary Science Reviews*, *78*, 169–187. https://doi.org/10.1016/j.quascirev.2013.08.006.

Robertson, J., Meschis, M., Roberts, G. P., Ganas, A., & Gheorghiu, D. M. (2019). Temporally constant Quaternary uplift rates and their relationship with extensional upper-plate faults in south Crete (Greece), constrained with 36Cl cosmogenic exposure dating. *Tectonics*, *38*(4), 1189–1222. https://doi.org/10.1029/2018TC005410.

Robertson, J., Roberts, G. P., Ganas, A., Meschis, M., Gheorghiu, D. M., & Shanks, R. P. (2023). Quaternary uplift of palaeoshorelines in southwestern Crete: the combined effect of extensional and compressional faulting. *Quat. Sci. Rev.*, *316*(108240), 108240. https://doi.org/10.1016/j.quascirev.2023.108240.

Robertson, J., Roberts, G. P., Iezzi, F., Meschis, M., Gheorghiu, D. M., Sahy, D., Bristow, C., & Sgambato, C. (2020). Distributed normal faulting in the tip zone of the South Alkyonides Fault System, Gulf of Corinth, constrained using 36Cl exposure dating of late-Quaternary wave-cut platforms. *J. Struct. Geol.*, *136*(104063), 104063. https://doi.org/10.1016/j.jsg.2020.104063.

Robustelli, G. (2019). Geomorphic constraints on uplift history in the Aspromonte Massif, southern Italy. *Geomorphology*, *327*, 319–337. https://doi.org/10.1016/j.geomorph.2018.11.011.

Roche, V., Camanni, G., Childs, C., Manzocchi, T., Walsh, J., Conneally, J., Saqab, M. M., & Delogkos, E. (2021). Variability in the three-dimensional geometry of segmented normal fault surfaces. *Earth-Science Reviews*, *216*(103523), 103523. https://doi.org/10.1016/j.earscirev.2021.103523.

Roda-Boluda, D. C., D'Arcy, M., McDonald, J., & Whittaker, A. C. (2018). Lithological controls on hillslope sediment supply: insights from landslide activity and grain size distributions. *Earth Surface Processes and Landforms*, *43*(5), 956–977. https://doi.org/10.1002/esp.4281.

Roda-Boluda, D. C., D'Arcy, M., Whittaker, A. C., Gheorghiu, D. M., & Rodés, Á. (2019). 10Be erosion rates controlled by transient response to normal faulting through incision and landsliding. *Earth and Planetary Science Letters*, *507*, 140–153. https://doi.org/10.1016/j.epsl.2018.11.032.

Roda-Boluda, D. C., & Whittaker, A. C. (2017). Structural and geomorphological constraints on active normal faulting and landscape evolution in Calabria, Italy. *Journal of the Geological Society*, *174*(4), 701–720. https://doi.org/10.6084/m9.figshare.c.3689464.

Rohais, S., Bailleul, J., Brocheray, S., Schmitz, J., Paron, P., Kezirian, F., & Barrier, P. (2021). Depositional Model for Turbidite Lobes in Complex Slope Settings Along Transform Margins: The Motta San Giovanni Formation (Miocene—Calabria, Italy). *Frontiers in Earth Science*, *9*(November), 1–23. https://doi.org/10.3389/feart.2021.766946.

Rohling, E. J., Foster, G. L., Grant, K. M., Marino, G., Roberts, A. P., Tamisiea, M. E., & Williams, F. (2014). Sea-level and deep-sea-temperature variability over the past 5.3 million years. *Nature*, *508*(7497), 477–482. https://doi.org/10.1038/nature13230.

Rosenbaum, G., & Lister, G. S. (2004). Neogene and Quaternary rollback evolution of the Tyrrhenian Sea, the Apennines, and the Sicilian Maghrebides. *Tectonics*, *23*(1). https://doi.org/10.1029/2003TC001518.

Rossetti, F., Faccenna, C., Goffé, B., Monié, P., Argentieri, A., Funiciello, R., & Mattei, M. (2001). Alpine structural and metamorphic signature of the sila piccola massif nappe stack (Calabria, Italy): Insights for the tectonic evolution of the calabrian arc. *Tectonics*, *20*(1), 112–133. https://doi.org/10.1029/2000TC900027.

Rotevatn, A., Jackson, C. A.-L., Tvedt, A. B. M., Bell, R. E., & Blækkan, I. (2019). How do normal faults grow? *J. Struct. Geol.*, *125*, 174–184. https://doi.org/10.1016/j.jsg.2018.08.005

Schildgen, T. F., Cosentino, D., Caruso, A., Buchwaldt, R., Yldrm, C., Bowring, S. A., Rojay, B., Echtler, H., & Strecker, M. R. (2012). Surface expression of eastern Mediterranean slab dynamics: Neogene topographic and structural evolution of the southwest margin of the Central Anatolian Plateau, Turkey. *Tectonics*, *31*(2). https://doi.org/10.1029/2011TC003021.

Serpelloni, E., Bürgmann, R., Anzidei, M., Baldi, P., Mastrolembo Ventura, B., & Boschi, E. (2010). Strain accumulation across the Messina Straits and kinematics of Sicily and Calabria from GPS data and dislocation modeling. *Earth and Planetary Science Letters*, *298*(3–4), 347–360. https://doi.org/10.1016/j.epsl.2010.08.005.

Sgambato, C., Faure Walker, J. P., Roberts, G. P., Mildon, Z. K., & Meschis, M. (2023). Influence of fault system geometry and slip rates on the relative role of coseismic and interseismic stresses on earthquake triggering and recurrence variability. *J. Geophys. Res. Solid Earth*, *128*(11). https://doi.org/10.1029/2023JB026496.

Siddall, M., Rohling, E. J., Almogi-Labin, A., Hemleben Ch and Meischner, D., Schmelzer, I., & Smeed, D. A. (2003). Sea-level fluctuations during the last glacial cycle. *Nature*, *423*(6942), 853–858. https://doi.org/10.1038/nature01690.

Spratt, R. M., & Lisiecki, L. E. (2016). A Late Pleistocene sea level stack. *Climate of the Past*, *12*(4), 1079–1092. https://doi.org/10.5194/cp-12-1079-2016.

Stewart, I. S., Cundy, A., Kershaw, S., & Firth, C. (1997). Holocene coastal uplift in the taormina area, northeastern sicily: Implications for the southern prolongation of the calabrian seismogenic belt. *J. Geodyn.*, *24*(1–4), 37–50. https://doi.org/10.1016/S0264-3707(97)00012-4.

Stewart, I. S., & Hancock, P. L. (1988). Normal fault zone evolution and fault scarp degradation in the Aegean region. *Basin Research*, *1*(3), 139–153. https://doi.org/10.1111/j.1365-2117.1988.tb00011.x.

Tarquini, S., Isola, I., Favalli, M., Battistini, A., & Dotta, G. (2023). *TINITALY, a digital elevation model of Italy with a 10 meters cell size (Version 1.1)*. https://tinitaly.pi.ingv.it/.

Tortorici, G., Bianca, M., De Guidi, G., Monaco, C., & Tortorici, L. (2003). Fault activity and marine terracing in the Capo Vaticano area (southern Calabria) during the Middle-Late Quaternary. In *Quaternary International*. https://doi.org/10.1016/S1040-6182(02)00107-6.

Tortorici, L., Monaco, C., Tansi, C., & Cocina, O. (1995). Recent and active tectonics in the Calabrian arc (Southern Italy). In *Tectonophysics* (Vol. 243). https://doi.org/10.1016/0040-1951(94)00190-K.

Tucker, G. E., Hobley, D. E. J., McCoy, S. W., & Struble, W. T. (2020). Modeling the shape and evolution of normal-fault facets. *J. Geophys. Res. Earth Surf.*, *125*(3).

Tucker, G. E., McCoy, S. W., Whittaker Alexander C and Roberts, G. P., Lancaster, S. T., & Phillips, R. (2011). Geomorphic significance of postglacial bedrock scarps on normal-fault footwalls. *J. Geophys. Res.*, *116*(F1).

van Hinsbergen, D. J. J., van der Meer, D. G., Zachariasse, W. J., & Meulenkamp, J. E. (2006). Deformation of western Greece during Neogene clockwise rotation and collision with Apulia. *International Journal of Earth Sciences*, *95*(3), 463–490. https://doi.org/10.1007/s00531-005-0047-5.

Varzi, A. G., Meschis, M., Fallati, L., Scicchitano, G., De Santis, V., Scardino, G., Basso, D., Bracchi, V. A., & Savini, A. (2024). New chronology for submerged relict paleoshorelines and associated rates of crustal vertical movements offshore the Marzamemi village, Sicily (Southern Italy). *Mar. Geol.*, *474*(107326), 107326. https://doi.org/10.1016/j.margeo.2024.107326.

Veliz-Borel, V., Mouslopoulou, V., Nicol, A., Begg, J., & Oncken, O. (2022). Normal Faulting Along the Kythira-Antikythira Strait, Southwest Hellenic Forearc, Greece. *Frontiers in Earth Science*, *9*(January). https://doi.org/10.3389/feart.2021.730806.

Violanti, D. (1989). Plio-Pleistocene foraminifera from northern side of Peloritani Mountains: biostratigraphic and paleoenvironmental analysis. *Rivista Italiana Paleontologia e Stratigrafia*, *95*(2), 173–216.

Violanti, D., Bonfiglio L., & Sacca' D. (1987). Pleistocene foraminifera and paleoenvironmental interpretations in an outcrop of NE Sicily (Rometta, Messina). *Rivista Italiana Paleontologia e Stratigrafia*, *93*(2), 251–286.

Vitale, S., & Ciarcia, S. (2013). Tectono-stratigraphic and kinematic evolution of the southern Apennines/Calabria-Peloritani Terrane system (Italy). *Tectonophysics*, *583*, 164–182. https://doi.org/10.1016/j.tecto.2012.11.004.

Wallace, R. E. (1977). Profiles and ages of young fault scarps, north-central Nevada. *Geol. Soc. Am. Bull.*, *88*(9), 1267. https://doi.org/10.1130/0016-7606(1977)88<1267:PAAOYF>2.0.CO;2.

Walsh, J. J., Childs, C., Meyer, V., Manzocchi, T., Imber, J., Nicol, A., Tuckwell, G., Bailey, W. R., Bonson, C. G., Watterson, J., Nell, P. A., & Strand, J. (2001). Geometric controls on the evolution of normal fault systems. *Geol. Soc. Spec. Publ.*, *186*(1), 157–170. https://doi.org/10.1144/GSL.SP.2001.186.01.10.

Westaway, R. (1993). Quaternary uplift of southern Italy. *Journal of Geophysical Research*, *98*(B12), 21,741-21,772. https://doi.org/10.1029/93jb01566.

Wortel, M. J. R., & Spakman, W. (2000). Subduction and Slab Detachment in the Mediterranean-Carpathian Region. *Science*, *290*, 1910–1917. https://doi.org/10.1126/science.290.5498.1910.

Zecchin, M., Praeg, D., Ceramicola, S., & Muto, F. (2015). Onshore to offshore correlation of regional unconformities in the Plio-Pleistocene sedimentary successions of the Calabrian Arc (central Mediterranean). In *Earth-Science Reviews* (Vol. 142, pp. 60–78). Elsevier. https://doi.org/10.1016/j.earscirev.2015.01.006.